HHS Public Access

Author manuscript

*Nature*. Author manuscript; available in PMC 2018 October 18.

Published in final edited form as:

*Nature*. 2018 April ; 556(7702): 520–524. doi:10.1038/s41586-018-0046-x.

# Structural basis of ligand binding modes at the neuropeptide Y $Y_1$ receptor

**Zhenlin Yang**[1,2,*], **Shuo Han**[1,3,*], **Max Keller**[4,*], **Anette Kaiser**[5,*], **Brian J. Bender**[6,*], **Mathias Bosse**[7], **Kerstin Burkert**[5], **Lisa M. Kögler**[5], **David Wifling**[4], **Guenther Bernhardt**[4], **Nicole Plank**[4], **Timo Littmann**[4], **Peter Schmidt**[7], **Cuiying Yi**[1], **Beibei Li**[1,8], **Sheng Ye**[3], **Rongguang Zhang**[3,9], **Bo Xu**[10], **Dan Larhammar**[10], **Raymond C. Stevens**[11,12], **Daniel Huster**[7], **Jens Meiler**[6,13], **Qiang Zhao**[1,2,8,14], **Annette G. Beck-Sickinger**[5], **Armin Buschauer**[4], and **Beili Wu**[1,8,12,14]

[1]CAS Key Laboratory of Receptor Research, Shanghai Institute of Materia Medica, Chinese Academy of Sciences, 555 Zuchongzhi Road, Pudong, Shanghai 201203, China

[2]State Key Laboratory of Drug Research, Shanghai Institute of Materia Medica, Chinese Academy of Sciences, 555 Zuchongzhi Road, Pudong, Shanghai 201203, China

[3]National Laboratory of Biomacromolecules, Institute of Biophysics, Chinese Academy of Sciences, Beijing 100101, China

[4]Pharmaceutical/Medicinal Chemistry II, Institute of Pharmacy, University of Regensburg, Universitätsstr. 31, D-93053 Regensburg, Germany

[5]Institute of Biochemistry, Faculty of Biosciences, Pharmacy and Psychology, Leipzig University, Brüderstr. 34, D 04103 Leipzig, Germany

[6]Department of Pharmacology, Center for Structural Biology, Vanderbilt University, 465 21st Ave South, Nashville, TN 37203, USA

[7]Institute of Medical Physics and Biophysics, Leipzig University, Härtelstrasse 16-18, 04107 Leipzig, Germany

[8]University of Chinese Academy of Sciences, No.19A Yuquan Road, Beijing 100049, China



Correspondence and requests for materials should be addressed to B.W. (beiliwu@simm.ac.cn), A.B. (Armin.Buschauer@chemie.uni-regensburg.de) or A.G.B.-S. (abeck-sickinger@uni-leipzig.de).

*These authors contributed equally to this work.

**Author Contributions** Z.Y. and S.H. optimized the construct, developed the purification procedure, purified the $Y_1R$ protein for crystallization, performed crystallization trials, solved the structures and wrote the manuscript. M.K., D.W., G.B., N.P. and T.L. sythesized the compounds, designed, performed and analysed ligand binding assay. A.K., K.B. and L.M.K. performed peptide sythesis, IP accumalation assays, photo-crosslinking assay and mass spectrometry after crosslinking. B.J.B. helped to refine the $Y_1R$–UR-MK299 structure and modelled the $Y_1R$–NPY complex. M.B. and P.S. performed and analysed NMR data. C.Y. expressed the $Y_1R$ proteins. B.L. helped with construct and crystal opimization. S.Y., R.Z., B.X., D.L., R.C.S., D.H., J.M., A.G.B.-S. and A.B. helped with structure analysis/interpretation and edited the manuscript. R.C.S. helped to initiate the project. D.H. oversaw NMR studies. J.M. oversaw molecular docking. Q.Z. collected X-ray diffraction data and solved the structures. A.G.B.-S. oversaw peptide synthesis, IP accumulation and photo-crosslinking assays. A.B. oversaw compound sythesis and ligand binding assays. B.W. and Q.Z. initiated the project, planned and analysed experiments, supervised the research, and wrote the manuscript with input from all co-authors.

The authors declare no competing financial interests. Readers are welcome to comment on the online version of the paper.

[9]National Center for Protein Science Shanghai, Institute of Biochemistry and Cell Biology, Shanghai Institutes for Biological Sciences, Chinese Academy of Sciences, Shanghai 201203, China

[10]Department of Neuroscience, Science for Life Laboratory, Uppsala University, Box 593, SE-751 24 Uppsala, Sweden

[11]iHuman Institute, ShanghaiTech University, 393 Hua Xia Zhong Road, Shanghai 201210, China

[12]School of Life Science and Technology, ShanghaiTech University, 393 Hua Xia Zhong Road, Shanghai 201210, China

[13]Departments of Chemistry and Bioinformatics, Center for Structural Biology, Vanderbilt University, 465 21st Ave South, Nashville, TN 37203, USA

[14]CAS Center for Excellence in Biomacromolecules, Chinese Academy of Sciences, Beijing 100101, China

## Abstract

Neuropeptide Y (NPY) receptors belong to the G protein-coupled receptor (GPCR) superfamily and play important roles in food intake, anxiety and cancer regulation[1,2]. The NPY/Y receptor system has emerged as one of the most complex networks with three peptide ligands (NPY, peptide YY and pancreatic polypeptide) binding to four receptors in mammals, namely $Y_1$, $Y_2$, $Y_4$ and $Y_5$ receptors, with different affinity and selectivity[3]. NPY is the most powerful stimulant of food intake and this effect is primarily mediated by $Y_1$ receptor ($Y_1R$)[4]. A number of peptides and small-molecule compounds have been characterized as $Y_1R$ antagonists and have shown clinical potential in the treatment of obesity[4], tumor[1] and bone loss[5]. However, their clinical usage has been hampered by low potency and selectivity, poor brain penetration ability or lack of oral bioavailability[6]. Here we report crystal structures of the human $Y_1R$ bound to two selective antagonists UR-MK299 and BMS-193885 at 2.7 and 3.0 Å resolution, respectively. The structures combined with mutagenesis studies reveal binding modes of $Y_1R$ to several structurally diverse antagonists and determinants of ligand selectivity. The $Y_1R$ structure and molecular docking of the endogenous agonist NPY, together with nuclear magnetic resonance (NMR), photo-crosslinking and functional studies, provide insights into the binding behavior of the agonist and for the first time determine the interaction of its N terminus with the receptor. These insights into $Y_1R$ can enable structure-based drug discovery targeting NPY receptors.

NPY is a highly abundant neuropeptide in the central nervous system[7]. The first characterized NPY receptor $Y_1R$ is widely expressed in a variety of tissues and involved in regulation of many physiological functions, related to obesity[8] and cancer[9]. To better understand the ligand binding behavior of NPY receptors and provide a basis for drug discovery, we solved crystal structures of $Y_1R$ in complex with two structurally diverse antagonists, UR-MK299, an argininamide with high $Y_1R$ selectivity[10], and BMS-193885, which displays anorectic activity in animal models[6] (Fig. 1 and Extended Data Table 1). To facilitate structure determination, an engineered $Y_1R$ construct was designed (see Methods).

Within the β-branch of class A GPCRs, to which NPY receptors belong, the structures of four receptors, namely the neurotensin receptor NTS1[11], the $OX_1$ and $OX_2$ orexin

receptors[12,13] and the endothelin $ET_B$ receptor[14], are determined to date. These structures reveal distinct differences of ligand binding modes between different receptors, suggesting that more structural information is needed to develop any consensus about the ligand recognition mechanisms for this GPCR subfamily. The $Y_1R$ structure shares a canonical seven transmembrane helical bundle (helices I-VII) with the other known GPCR structures (Fig. 1 and Extended Data Fig. 1a, b). The $Y_1R$–UR-MK299 and $Y_1R$–BMS-193885 complexes are structurally similar with $C_\alpha$ root-mean-square deviation (r.m.s.d.) of 0.75 Å within the helical bundle, and both exhibit inactive conformations with helix VI adopting a similar inward conformation as that in the other inactive GPCR structures. UR-MK299 binds to $Y_1R$ in a cavity within the helical bundle bordered by helices III, IV, V, VI and VII (Fig. 2a, b). The diphenylmethyl moiety of the antagonist interacts with a hydrophobic cluster formed by $F282^{6.54}$, $F286^{6.58}$ and $F302^{7.35}$ (superscript: Ballesteros-Weinstein nomenclature[15]) on helices VI and VII of $Y_1R$. The critical role of this hydrophobic patch in recognizing the argininamide-type $Y_1R$ antagonist was confirmed by the NPY-induced inositol phosphate (IP) accumulation of $Y_1R$ inhibited by UR-MK299 and several related $Y_1R$ antagonists, BIBP3226, BIBO3304, UR-HU404 and UR-MK289 (Extended Data Fig. 1e-i). The mutation $F302^{7.35}A$ abolishes the antagonistic activity for all these antagonists, while a 2-5-fold decreased antagonistic effect of all tested antagonists was observed for $F286^{6.58}A$ (Fig. 3a-c, Extended Data Fig. 2 and Extended Data Table 2).

The hydroxyphenyl group of UR-MK299 sits in a groove formed by helices III and VI of the receptor, enabling hydrophobic contacts with residues $Q120^{3.32}$, $C121^{3.33}$, $I124^{3.36}$, $W276^{6.48}$ and $L279^{6.51}$. In $Y_1R$ and $Y_2R$, $Q120^{3.32}$ is suggested to be the interaction partner for the C terminus of NPY and crucial for receptor activation[16]. In the $Y_1R$–UR-MK299 structure, this residue forms a hydrophobic contact with the phenyl ring of the hydroxyphenyl group in UR-MK299, potentially blocking the binding of $Y_1R$ to NPY. Mutagenesis data show that the mutation $Q120^{3.32}N$ does not influence the inhibitory effect of $Y_1R$ antagonists on NPY signalling, but a replacement to histidine dramatically increases antagonistic activity of these ligands (Fig. 3d, e and Extended Data Table 2), suggesting that an additional π-stacking interaction with the antagonist is beneficial at this position. The highly conserved residue $W^{6.48}$ represents the so-called “toggle switch” and was suggested to trigger receptor activation through a conformational change in various GPCRs[17]. In the $Y_1R$–UR-MK299 structure, the residue $W276^{6.48}$ is in a conformation similar to those observed in other inactive class A GPCR structures and distinct from their active-state conformations[18,19]. The hydroxyphenyl group of UR-MK299 forms a hydrophobic contact with $W276^{6.48}$, potentially preventing its activation-related motion and stabilizing the receptor in an inactive conformation. Compared to the wild-type receptor, the $Y_1R$ mutant $W276^{6.48}A$ displayed an over 2,000-fold decrease in binding affinity to [$^3$H]-UR-MK299 (Extended Data Table 3) and reduced the antagonistic activity of the argininamide-type $Y_1R$ antagonists by 4-7 fold (Fig. 3f and Extended Data Table 2), supporting its important role in antagonist recognition.

Residues $N283^{6.55}$ and $D287^{6.59}$ were suggested as the most important amino acids for $Y_1R$ ligand recognition[20]. In the $Y_1R$–UR-MK299 structure, $N283^{6.55}$ is engaged in two hydrogen bonds with the alpha-nitrogen and the carboxylic oxygen of arginine in UR-MK299. $D287^{6.59}$ builds a salt bridge with the protonated guanidinyl moiety and a hydrogen

bond with the carbamoyl group, in agreement with a decrease in antagonist affinity when the carbamoyl group was replaced by an alkoxycarbonyl, acyl or alkyl group[21]. The mutants N283$^{6.55}$A and D287$^{6.59}$N displayed a dramatic loss of NPY-induced receptor function and a complete abolishment of antagonistic activity for the small-molecule antagonists (Fig. 3g, h and Extended Data Table 2), which go along with an over 2,000-fold decreased binding affinity of $Y_1$R to [$^3$H]-UR-MK299 (Extended Data Table 3). These data indicate the critical roles of these two residues in agonist- and antagonist-binding. Additionally, the carbamoyl substituent at the guanidine group binds deep in a sub-pocket shaped by helices V and VI, characterized by hydrophobic contacts with L216$^{5.43}$, T280$^{6.52}$ and N283$^{6.55}$, and a hydrogen bond between the oxygen of the propionyl group and Q219$^{5.46}$. The latter was reflected by a 30-fold decrease in binding affinity of [$^3$H]-UR-MK299 to the $Y_1$R mutants Q219$^{5.46}$A and Q219$^{5.46}$V (Extended Data Table 3). Extra empty space at the bottom of the sub-pocket is observed in the $Y_1$R–UR-MK299 structure, suggesting that a larger substituent may be allowed (Extended Data Fig. 1c). This is supported by studies showing that some other carbamoylated argininamide-type $Y_1$R antagonists containing longer carbamoyl chains, such as UR-MK136 (Extended Data Fig. 1j), bind to the receptor with a relatively high affinity[10].

UR-MK299 was reported to exhibit high $Y_1$R selectivity ($Y_2$R: $K_i$>3,000 nM, $Y_4$R/$Y_5$R: $K_i$>10,000 nM) and specificity compared to two related neuropeptide FF (NPFF) receptors (NPFF$_1$R: $K_i$=1,000 nM; NPFF$_2$R: $K_i$>3,000 nM)[10]. Sequence alignment reveals that most of the key residues involved in UR-MK299 binding are conserved between $Y_1$R, the other NPY receptors and the NPFFRs, except for F$^{4.60}$, Q$^{5.46}$, N$^{6.55}$ and F$^{6.58}$ (Extended Data Fig. 3), indicating the importance of these four residues in terms of selectivity and specificity of UR-MK299. $Y_2$R is the only NPY receptor with L$^{5.46}$ instead of Q$^{5.46}$, preventing key polar contacts. In $Y_4$R, E$^{6.58}$ disturbs the F$^{6.54}$/F$^{6.58}$/F$^{7.35}$ hydrophobic patch and most likely mediates selectivity, supported by the F$^{6.58}$E mutation in $Y_1$R dramatically reducing binding affinity for BIBP3226[22], which contains the same diphenylmethyl group as UR-MK299. Similarly, hydrophilic residues at key positions impede high-affinity binding at $Y_5$R (T$^{6.58}$) and NPFF$_2$R (S$^{6.58}$), while the hydrophobic pocket is preserved though with less bulk in NPFF$_1$R (L$^{6.54}$/I$^{6.58}$/F$^{7.35}$), leading to moderate affinity of BIBP3226 ($K_i$=18 nM)[10].

The ligand BMS-193885 occupies a similar binding pocket as UR-MK299 within the helical bundle of $Y_1$R (Fig. 2c, d and Extended Data Fig. 1k). The dihydropyridine group fits in a sub-pocket formed by helices III, V and VI, which aligns with previous structure-activity relationship (SAR) studies showing that larger substituents at the position 3 of the dihydropyridine ring dramatically reduced $Y_1$R binding affinity[23]. Residue T280$^{6.52}$ forms a hydrogen bond with the nitrogen of the dihydropyridine ring as confirmed by our mutagenesis studies showing that the mutation T280$^{6.52}$A decreased the binding affinity of BMS-193885 by about 330 fold (Extended Data Table 3) and reported for a lower affinity N-methylated derivative[24]. Additionally, the dihydropyridine ring makes a hydrophobic contact with residue I124$^{3.36}$, which is consistent with a 400-fold decrease in affinity at the mutant I124$^{3.36}$A (Extended Data Table 3). It was also reported that methylation of either nitrogen of the urea group of BMS-193885 significantly decreased binding ability of the methylated derivatives to $Y_1$R[24], suggesting that these hydrogen-bond donors are critical for $Y_1$R recognition. Indeed, in the BMS-193885-bound $Y_1$R structure, the urea group forms

hydrogen bond interactions with D287$^{6.59}$. Similar to the diphenylmethyl group of UR-MK299, the piperidine and methoxyphenyl rings of BMS-193885 form extensive hydrophobic contacts with the residues F282$^{6.54}$, F286$^{6.58}$ and F302$^{7.35}$. Replacement of the methoxyphenyl substituent by piperidine resulted in lower binding affinity to $Y_1R$[23], indicating the importance of the methoxyphenyl group in $Y_1R$ binding and reflecting lipophilic demands at this position.

Understanding the binding mode of the endogenous agonist NPY at a molecular level will facilitate the rational development of $Y_1R$ selective ligands. The C-terminal pentapeptide of NPY was identified to be essential for binding to the NPY receptors[25]. Since the hydroxyphenyl and the argininamide group of UR-MK299 mimic R35 and Y36 in the C terminus of NPY (Extended Data Fig. 1l), the crystal structure of $Y_1R$–UR-MK299 serves as a good template for molecular docking of the agonist. To aid docking, complementary mutagenesis studies were performed to determine corresponding interaction partners between $Y_1R$ and NPY (Extended Data Table 4a). Furthermore, solid-state NMR chemical shift measurements revealed residue-specific alterations of the secondary structure of NPY upon binding to $Y_1R$ (Extended Data Fig. 4). A number of key $Y_1R$/NPY contacts identified by the mutagenesis studies were used to guide NPY docking in Rosetta[26] with the final models being filtered against the NMR data to generate a final ensemble that best represents the combined data. The NPY-bound model reveals a relatively flat binding pose of NPY to $Y_1R$ with the C-terminal tetrapeptide R33-Y36, identified as a random coil/β-strand structure in NMR, penetrating into the binding pocket (Fig. 4a). The unstructured N terminus, Y1-P13, is in close proximity to the second extracellular loop (ECL2), while the α-helix in the middle region of NPY, A14-T32, lays along ECL1 and ECL3 and points away from ECL2.

Inspection of the NPY binding pocket shows a similar binding pose of NPY's residue R35 as the argininamide of UR-MK299 (Fig. 4b). R35 forms a salt bridge with the residue D287$^{6.59}$ of $Y_1R$ and approaches to N283$^{6.55}$ (Fig. 4c). The NPY mutant R35A displays an over 6,000-fold decrease in activity and represents the highest influence on agonist potency of all tested NPY analogues (Extended Data Table 4a), supporting the importance of the positively charged residue in NPY recognition. D/E is not found at position 6.59 in any peptide GPCRs except for the receptors that bind to RF-amide peptides, including NPFF, prolactin releasing peptide and pyroglutamylated Arg-Phe-amide peptide, which share a common C-terminal Arg-Phe-$NH_2$ motif, supporting the hypothesis that the arginine may function similarly as R35 of NPY by interacting with the conserved D/E$^{6.59}$ of the respective receptors[27]. In contrast to the similar binding mode between R35 of NPY and the guanidine group of UR-MK299, the C-terminal tyrosinamide of NPY and the hydroxyphenyl group of UR-MK299 show different orientations. The hydroxyphenyl ring is oriented towards helix V (Q219$^{5.46}$) in the UR-MK299-bound $Y_1R$ structure, while Y36 of NPY points toward the residue Q120$^{3.32}$ on helix III in the NPY-docked model (Fig. 4c). This may arise from the opposite configuration of the stereo center in R35 of NPY and UR-MK299, as well as by only partial mimicking of the Y36-$NH_2$ of NPY by a 4-hydroxybenzyl group in UR-MK299 (Extended Data Fig. 1g, l). In the $Y_1R$–UR-MK299 structure, residue Q120$^{3.32}$ forms a hydrophobic contact with the hydroxyphenyl group of the antagonist. In contrast, the NPY-bound model shows that side chain of Q120$^{3.32}$ points almost in the opposite direction and

engages in a hydrogen bond with the hydroxy group of Y36-$NH_2$ (Extended Data Fig. 1d), similar as the interaction between the $Y_2R$ residue $Q^{3.32}$ and NPY suggested by Xu *et al.*[28] In $Y_2R$, it was also reported that $Q^{3.32}$ may interact with the C-terminal amide of NPY[16]. IP accumulation studies show that the $Y_1R$ mutation $Q120^{3.32}H$ leads to a 26-fold decrease in potency of NPY, and NPY-tyramide lacking the C-terminal amide displays a 45-fold loss of activity. Complementary mutagenesis revealed an additional reduction of NPY-tyramide potency at the mutant $Q120^{3.32}H$, and thus rules out a direct contact between the C-terminal amide of NPY and $Q120^{3.32}$ in $Y_1R$ (Extended Data Table 4a). Additionally, Y36 of NPY forms hydrophobic contacts with $Y100^{2.64}$ and $W106^{2.70}$ in $Y_1R$ (Fig. 4c). Although $Y100^{2.64}$ is not involved in antagonist binding, mutagenesis data suggest a critical role in agonist recognition as the $Y_1R$ mutant $Y100^{2.64}A$ displays a 284-fold decrease in potency for NPY (Fig. 3i and Extended Data Table 2). Furthermore, the model reveals close contacts between L30 of NPY and I293 in ECL3 of $Y_1R$ and between R33 of NPY and the $Y_1R$ residue $N299^{7.32}$ (Fig. 4c), which align with complemetary mutagenesis data showing no further loss of function for combining mutant I293N with $[N^{30}]$NPY and $N299^{7.32}A$ with $[A^{33}]$NPY (Fig. 3j-m and Extended Data Table 4a).

Previous studies showed different behaviors of the NPY receptors binding to the N terminus of NPY. While $Y_2R$ and $Y_5R$ can bind to N-terminally truncated NPY, $Y_1R$ and $Y_4R$ require the complete N terminus of NPY for full agonist potency[25,27]. However, these data did not allow conclusions about the interaction of the N terminus of NPY with the receptor. To further explore an involvement of NPY's N terminus in receptor-ligand recognition, we performed mutagenesis studies, showing that truncation of the first two residues of NPY (NPY(3-36)) reduces peptide potency by more than 50 fold (Extended Data Table 4b). This decrease in potency, however, is not seen when these residues are mutated to alanine ($[A^1,A^2]$NPY: 5-fold $EC_{50}$ shift), suggesting important contributions of peptide backbone in binding to the receptor. Our NPY-bound model suggests that the N-terminal region of NPY makes close contacts with the fragment T180-F199 in ECL2 of $Y_1R$ and is also in proximity to the receptor N terminus (Fig. 4a, d). To experimentally verify interacting sites in the receptor, we performed photo-crosslinking studies between NPY analogues carrying the highly reactive *p*-benzoyl-phenylalanine $[Bpa^1, K^4[(Ahx)_2$-biotin$]]$NPY and $Y_1R$. Crosslinked fragments were assigned to two regions in $Y_1R$, the N terminus (K21-D32) and ECL2 (A191-D205) (Extended Data Fig. 5 and Extended Data Table 5). Previous studies demonstrated that deletion of the $Y_1R$ N terminus does not interfere with receptor signalling, but reduces NPY binding by about 95% compared to the full-length receptor[29]. This creates the possibility that the N terminus of $Y_1R$ plays a role in recognizing and positioning the peptide ligand, which aligns with the photo-crosslinking data. Consistent with the crosslinking hits in receptor ECL2, our mutagenesis data show that mutations F184A/N and V197N in this region greatly reduce NPY potency (Extended Data Table 4c). Together, these data suggest that the N terminus and ECL2 of $Y_1R$ play important roles in recognition of NPY's N terminus and receptor activation. This contrasts with NPY binding at $Y_2R$, in which ECL2 may interact with the central α-helix of NPY and the peptide N terminus is flexible and unanchored by the receptor[16]. Whereas this study provides insights into the interactions between $Y_1R$ and NPY, further structural details, such as the structures of Y

receptors bound to NPY, are required to fully understand the endogenous agonist binding modes of the NPY receptor family.

## Methods

### Cloning and protein expression

DNA sequence of wild-type human $Y_1R$ was optimized and synthesized by Genewiz and then cloned into a modified **pFastBac1** vector (Invitrogen), which contains an expression cassette with a haemagglutinin (HA) signal sequence followed by a Flag tag prior to the receptor at the N terminus and a PreScission protease site followed by a 10×His-tag at the C terminus. An engineered construct was generated by inserting a modified T4 Lysozyme (T4L)[31] at the third intracellular loop (ICL3) between residues R241 and D250 and introducing a mutation $F129^{3.41}W$[32]. Twenty-five amino acids (V359-I384) were truncated at the C terminus to further improve protein yield and stability. Bac-to-Bac Baculovirus Expression System (Invitrogen) was used to generate high-titer (>$10^8$ viral particles per ml) recombinant baculovirus. *Spodoptera frugiperda* (*Sf*9) cells (Invitrogen) at density of 2 × $10^6$ cells per ml were infected by viral stock at MOI (multiplicity of infection) of 5. In company with the virus, a ligand (UR-MK299 or BMS-193885) was added to the cell culture to a final concentration of 1 μM. Transfected cells were cultured at 27 ºC for 48 h and then collected by centrifugation and stored at −80 ºC until use.

### Purification of $Y_1R$–UR-MK299 and $Y_1R$–BMS-193885 complexes

Frozen insect cells expressing the $Y_1R$–UR-MK299 complex were disrupted with thawing and repeated dounce homogenization in a hypotonic buffer containing 10 mM HEPES, pH 7.5, 10 mM $MgCl_2$, 20 mM KCl and protease inhibitor cocktail (Roche). After centrifugation at 160,000 *g* for 30 min, cell debris was re-suspended in a high osmotic buffer (10 mM HEPES, pH 7.5, 1 M NaCl, 10 mM $MgCl_2$, 20 mM KCl) followed by extensive homogenization. Soluble and membrane associated proteins were removed from the suspension by centrifugation. This procedure was repeated for 2-3 more times and then the hypotonic buffer was used to remove the high concentration of NaCl. Purified membranes were re-suspended in the hypotonic buffer with additional 30% (v/v) glycerol and stored at −80 ºC until use.

Purified membranes were thawed on ice in the presence of 100 μM UR-MK299, 2 mg $ml^{-1}$ iodoacetamide (Sigma) and EDTA-free protease inhibitor cocktail (Roche) and incubated at 4 ºC for 1 h. Equal volume of solubulization buffer containing 100 mM HEPES, pH 7.5, 1 M NaCl, 1% (w/v) n-dodecyl-b-D-maltopyranoside (DDM, Anatrace), 0.2% (w/v) cholesterol hemisuccinate (CHS) (Sigma) was added and incubation was continued for additional 3 h. The supernatant was isolated by centrifugation at 160,000 *g* for 30 min and incubated with TALON resin (Clontech) supplemented with 10 mM imidazole, pH 7.5 at 4 ºC overnight. The resin was then washed with ten column volumes of 25 mM HEPES, pH 7.5, 500 mM NaCl, 0.05% (w/v) DDM, 0.01% (w/v) CHS, 10% (v/v) glycerol, 30 mM imidazole and 50 μM UR-MK299, followed by ten column volumes of 50 mM HEPES, pH 7.5, 500 mM NaCl, 0.05% (w/v) DDM, 0.01% (w/v) CHS, 10% (v/v) glycerol, 10 mM $MgCl_2$, 5 mM ATP and 50 μM UR-MK299 and five column volumes of 25 mM HEPES, pH 7.5, 500 mM

NaCl, 0.05% (w/v) DDM, 0.01% (w/v) CHS, 10% (v/v) glycerol and 50 μM UR-MK299. The protein was eluted by five column volumes of 25 mM HEPES, pH 7.5, 500 mM NaCl, 0.05% (w/v) DDM, 0.01% (w/v) CHS, 10% (v/v) glycerol, 300 mM imidazole and 100 μM UR-MK299. A PD MiniTrap G-25 column (GE healthcare) was used to remove imidazole. The C-terminal His-tag and glycosylation was then treated by overnight digestion with His-tagged PreScission protease (custom-made) and His-tagged PNGase F (custom-made). Ni-NTA super flow resin (Qiagen) reverse binding was performed to remove the PreScission protease, PNGase F and the cleaved His-tag. The purified $Y_1$R–UR-MK299 complex was collected and concentrated to 20-30 mg $ml^{-1}$ with a 100 kDa molecular weight cutoff concentrator (Sartorius Stedim Biotech). Receptor purity and monodispersity were estimated by SDS-PAGE and analytical size-exclusion chromatography (aSEC).

The $Y_1$R–BMS-193885 complex protein was purified following the same procedure as above. The membranes of $Y_1$R construct were incubated with 50 μM BMS-193885, 2 mg $ml^{-1}$ iodoacetamide (Sigma), and EDTA-free protease inhibitor cocktail (Roche) at 4 ºC for 1 h, and then solubilized in final concentration of 50 mM HEPES, pH 7.5, 500 mM NaCl, 0.5% (w/v) DDM, 0.1% (w/v) CHS, 10% glycerol and 25 μM BMS-193885 at 4 ºC for 3 h. The solubilized $Y_1$R–BMS-193885 complex bound to the TALON resin was washed with ten column volumes of 25 mM HEPES, pH 7.5, 500 mM NaCl, 0.05% (w/v) DDM, 0.01% (w/v) CHS, 10% (v/v) glycerol, 30 mM imidazole and 25 μM BMS-193885, followed by ten column volumes of 50 mM HEPES, pH 7.5, 500 mM NaCl, 0.05% (w/v) DDM, 0.01% (w/v) CHS, 10% (v/v) glycerol, 10 mM $MgCl_2$, 5 mM ATP and 25 μM BMS-193885 and five column volumes of 25 mM HEPES, pH 7.5, 500 mM NaCl, 0.05% (w/v) DDM, 0.01% (w/v) CHS, 10% (v/v) glycerol and 25 μM BMS-193885. The protein was eluted by five column volumes of 25 mM HEPES, pH 7.5, 500 mM NaCl, 0.05% (w/v) DDM, 0.01% (w/v) CHS, 10% (v/v) glycerol, 300 mM imidazole and 50 μM BMS-193885. The eluted sample was concentrated and desalted using the PD MiniTrap G-25 column (GE healthcare). Overnight digestion by Precission protease and PNGase F and Ni-NTA reverse binding were then performed to further purify the protein. The complex protein was concentrated to 10-20 mg $ml^{-1}$ and analyzed by SDS-PAGE and aSEC.

### Lipidic cubic phase crystallization of antagonist-bound $Y_1$Rs

The $Y_1$R sample in complex with UR-MK299 or BMS-193885 was mixed with molten lipid (monoolein/cholesterol 10:1 by mass) at a weight ratio of 1:1.5 (protein:lipid) using two syringes to create lipidic cubic phase (LCP). The mixture was dispensed onto glass sandwich plates (Shanghai FAstal BioTech) in 40 nl drop and overlaid with 800 nl precipitant solution using a Gryphon robot (Art-Robbins). Protein reconstitution in LCP and crystallization trials were performed at room temperature (19-22 ºC). Plates were placed in an incubator (Rock Imager, Formulatrix) and imaged at 20 ºC automatically following a schedule. Crystals of $Y_1$R–UR-MK299 complex showed up after 4 days and grew to the full size (150 × 50 × 5 $μm^3$) within two weeks in 0.1 M Tris, pH 7.4-8.0, 30-40% (v/v) PEG400, 50-150 mM sodium tartrate and 100 μM UR-MK299. The $Y_1$R–BMS-193885 complex was crystallized in 0.1 M HEPES, pH 7.2-7.6, 20% PEG400 and 50 μM BMS-193885 with the maximum size of 30 × 10 × 5 $μm^3$. The crystals of $Y_1$R–UR-MK299 and $Y_1$R–

BMS-193885 complexes were harvested directly from LCP using 150 μm and 50 μm micro mounts (M2-L19-50/100, MiTeGen), respectively, and flash frozen in liquid nitrogen.

## Data collection and structure determination

X-ray diffraction data were collected at the SPring-8 beam line 41XU, Hyogo, Japan, on a Pilatus3 6M detector (X-ray wavelength 1.0000 Å). Crystals were exposed with a 10 μm × 8 μm mini-beam for 0.2 s and 0.2° oscillation per frame. Data from 47 best-diffracting crystals of the $Y_1$R–UR-MK299 complex and 33 crystals of the $Y_1$R–BMS-193885 complex were processed by XDS[33], respectively. Structure of the $Y_1$R–UR-MK299 complex was solved by molecular replacement (MR) implemented in Phaser[34] using the receptor portion of NTSR1 (PDB ID: 4GRV), converted to polyalanines, and T4L structure (PDB ID: 1C6P) as search models. The correct MR solution contained one $Y_1$R-T4L molecule in the asymmetric unit. Initial refinement was performed with REFMAC5[35] and BUSTER[36], and then manual examination and rebuilding of the refined coordinates were carried out in COOT[37] using both |2Fo| – |Fc| and |Fo| – |Fc| maps. The structure has been carefully refined and the ramachandran plot analysis indicates that 100% of the residues are in favorable (95.5%) or allowed (4.5%) regions (no outliers). The final model includes 312 residues (F18-R241 and D250-F337) of the 384 residues of $Y_1$R and residues N2-Y161 of T4L. The $Y_1$R–BMS-193885 complex structure was solved using $Y_1$R in the $Y_1$R–UR-MK299 complex and T4L as search models and refined under the same procedure. The ramachandran plot analysis indicates that 100% of the residues are in favorable (95.4%) or allowed (4.6%) regions (no outliers). The final model of the $Y_1$R–BMS-193885 complex contains 301 residues (D31-R241 and D250-D339) of $Y_1$R and the 160 residues of T4L. Helix VIII in the $Y_1$R–UR-MK299 structure rotates towards helix VI by about 90° compared to that in the BMS-193885-bound structure most likely due to crystal packing (Extended Data Fig. 1).

## Immunoblotting

Total solublized protein of *Sf*9 membrane preparations (see above) used in radio ligand binding assay was determined by the Bradford method according to the manufacturers' protocol (BioRad Protein Assay; BioRad, Munich, Germany). Aliquots of homogenized membrane preparations, corresponding to 100 μg of protein, were centrifuged at 50,000 *g* at 4 °C for 15 min, and the pellets were re-suspended in 50 mM Tris, pH 7.4, supplemented with 1 mM EDTA and protease inhibitors (SIGMAFAST Protease Inhibitor cocktail tablets, Sigma) at a protein concentration of 1,600 μg $ml^{-1}$. Membrane homogenates (15 μl) were processed and subjected to immunoblotting as described previously[38] with the following modifications: blotting onto the nitrocellulose membrane was performed at 60 mA for 60 min. Primary antibody ANTI-FLAG M1 from mouse (Sigma, order no. F3040, lot SLBK1592V) was diluted 1:500. The secondary antibody, an anti-mouse IgG HRP-conjugated antibody from goat (Sigma, order no. A0168, lot 080M4839) was diluted 1:80,000. The washing steps after incubation with the primary and the secondary antibody were 3 × 10 min each. Control experiments in the absence of the primary antibody were not performed.

### Radio ligand binding assay

All binding experiments with [$^3$H]-UR-MK299 (synthesis described elsewhere[10]) were performed at *Sf9* membrane preparations in PP 96-well microplates (Greiner bio-one) at 23±1 °C using a sodium-containing, iso-osmotic HEPES buffer (10 mM HEPES, pH 7.4, 150 mM NaCl, 5 mM KCl, 2.5 mM $CaCl_2$, 1.2 mM $KH_2PO_4$, 1.2 mM $Mg_2SO_4$ and 25 mM $NaHCO_3$ supplemented with 1% BSA) for competition binding studies with antagonists, and a sodium-free, hypo-osmotic HEPES buffer (25 mM HEPES, pH 7.4, 2.5 mM $CaCl_2$ and 1 mM $MgCl_2$ supplemented with 1% BSA) for competition binding studies with the agonist NPY (in the following, both buffers are referred to as 'binding buffer'). Prior to competition binding experiments, $K_d$ values of [$^3$H]-UR-MK299 were determined by saturation binding using the respective binding buffer. In case of saturation binding experiments, [$^3$H]-UR-MK299 was 1:1 diluted with 'cold' UR-MK299 (in the following, the mixture is referred to as 'radioligand'). On the day of the experiment, *Sf*9 membranes were thawed and re-suspended using a 1-ml syringe equipped with a needle (20G) followed by centrifugation at 16,000 *g* at 4 °C for 10 min. The supernatant was discarded and the pellets were re-suspended in binding buffer using a 1-ml syringe equipped with a needle (27G3/4). The membrane homogenates were stored on ice until use. The total amount of protein per well was between 0.25 and 8 μg, depending on the receptor expression level.

Saturation binding experiments: for the determination of total binding, wells were pre-filled with binding buffer (160 μl), followed by the addition of binding buffer (20 μl), containing the radioligand at a 10-fold higher concentration compared to the final concentration. For the determination of unspecific binding (in the presence of UR-MK299 at a 100-fold excess), wells were pre-loaded with binding buffer (140 μl), binding buffer (20 μl) containing UR-MK299 (10-fold concentrated) and binding buffer (20 μl) containing the radioligand (10-fold concentrated). To all wells, 20 μl of the membrane suspension were added, and the plates were shaken at 23 °C for 90 min. The membranes were collected on GF/C filter mats (0.26 mm; Whatman, Maidstone, UK) (pre-treated with 0.3% polyethylenimine for 30 min) and washed with cold Tris buffer (91 g $l^{-1}$ Tris base, 25.5 g $l^{-1}$ $MgCl_2 \cdot 6H_2O$ and 3.76 g $l^{-1}$ EDTA) using a Brandel Harvester (Brandel, Gaithersburg, MD). Filter pieces were punched out and transferred into 1450-401 96-well plates (PerkinElmer, Rodgau, Germany). Rotiscint eco plus (Carl Roth, Karlsruhe, Germany) (200 μl) was added, and the plates were sealed with transparent tape (permanent seal for microplates, PerkinElmer), vigorously shaken for at least 3 h, and kept in the dark for at least 1 h prior to the measurement of radioactivity (dpm) with a MicroBeta2 plate counter (PerkinElmer). Specific binding data (dpm) were plotted against the free radioligand concentration in nM (obtained by subtracting the amount of bound radioligand (nM) (calculated from the specifically bound radioligand in dpm, the specific activity, and the volume per well) from the total radioligand concentration (nM)) and analyzed by a two-parameter equation describing hyperbolic binding (SigmaPlot 11.0, Systat Software Inc., Chicago, IL) to obtain $K_d$ and $B_{max}$ values. In case of $K_d$ values < 1 nM, the $B_{max}$ was kept below 1,200 dpm by choosing an appropriate protein concentration. In case of $K_d$ values > 1 nM, the $B_{max}$ was kept below 3,300 dpm.

Competition binding experiments were performed according to the procedure for saturation binding with the following modifications: [$^3$H]-UR-MK299 was used undiluted and in case

of $Y_1R$ mutants, at which [$^3$H]-UR-MK299 exhibited a $K_d$ value > 3 nM, the total volume per well was 100 µl, i.e., in the case of total binding, wells were pre-filled with binding buffer (80 µl), followed by the addition of binding buffer (10 µl) containing [$^3$H]-UR-MK299 (10-fold concentrated), and the membrane homogenate (10 µl). The following concentrations of [$^3$H]-UR-MK299 were used for competition binding with antagonists: 0.2 nM (wild-type $Y_1R$, T280$^{6.52}$A, T212$^{5.39}$A), 0.3 nM (F173$^{4.60}$W), 1.1 nM (L279$^{6.51}$A), 5 nM (Q219$^{5.46}$A), 7 nM (L215$^{5.42}$G), 10 nM (I124$^{3.36}$A, F173$^{4.60}$A). 1 nM [$^3$H]-UR-MK299 was used for competition binding with NPY. The incubation time was 90 min throughout. Unspecific binding was determined in the presence of UR-MK299 (100-fold excess to [$^3$H]-UR-MK299). Total binding was between 700 and 3,500 dpm. Maximum unspecific binding amounted to ≤ 30% of total binding. Specific binding data (dpm) were plotted against log (concentration competitor) and analyzed by a four-parameter logistic equation (log(inhibitor) vs response – variable slope, GraphPad Prism Software 5.0, GraphPad Software, San Diego, CA) to obtain $pIC_{50}$ values, which were converted to $IC_{50}$ values. In case of incomplete displacement of [$^3$H]-UR-MK299 (specifically bound radioligand at the highest competitor concentration between 20% and 50%), $pIC_{50}$ values were determined by plotting $\log(B/(B_0\text{-}B))$ (Hill plot; B = specifically bound radioligand in the presence of competitor (values between 10 and 90%), $B_0$ = specifically bound radioligand in the absence of competitor ($B_0$ = 100%)) against log(competitor concentration) (at least three data points) and $pIC_{50}$ values ($\log(B/(B_0\text{-}B)) = 0$) were determined by linear regression. $K_i$ values were calculated from the $IC_{50}$ value as well as the respective $K_d$ value (Extended Data Table 3) and the concentration of [$^3$H]-UR-MK299 according to the Cheng-Prusoff equation[39].

## IP accumulation assay

The signal transduction assay was performed as previously described[40,41]. Briefly, COS-7 cells (obtained from American Type Culture Collection) were seeded into 48-well plates and were transiently co-transfected with wild-type receptor or receptor mutant and a chimeric G protein ($G_{\alpha\Delta 6qi4myr}$) plasmid DNA[42]. Cells were routinely tested for mycoplasma contamination. Cells were radioactively labelled with myo-[2-$^3$H]-Inositol (Perkin Elmer, Boston, USA) overnight, and then stimulated with an increased concentration of NPY (NPY-curve). For antagonist curves, cells were stimulated with the antagonist (BIBP3226: $10^{-5}$ M, BIBO3304: $10^{-6}$ M, MK-HU404: $10^{-7}$ M, UR-MK289: $10^{-5}$ M, UR-MK299: $10^{-7}$M) parallel to an increased concentration of NPY for 1h (standard conditions). After cell lysis, an anion exchange chromatography was performed and isolated, radioactive accumulated IP derivatives were analyzed by liquid scintillation counting (scintillation cocktail Optiphase HiSafe, Perkin Elmer).

Using GraphPad Prism 5.0 (GraphPad Software, San Diego, CA, USA) the determined concentration response-curves were analyzed. The curves were normalized to the top (100%) and bottom (0%) values of the associated NPY curve. All curves of independent experiments were summarized to one single concentration response-curve by the row means total function. Using nonlinear regression (curve fit) the $EC_{50}$ and $pEC_{50}$ ± SEM were examined. The shift between NPY and NPY/antagonist curve is defined as $EC_{50}$ ratio and calculated by dividing $EC_{50(NPY/antagonist)}/EC_{50(NPY)}$, set Hill slope to 1. All experiments were performed in duplicates of at least two independent experiments.

### Live cell fluorescence microscopy

The membrane localization of $Y_1R$ and receptor mutants was verified by fluorescence microscopy. COS-7 cells were seeded in 8 well μ-slides (IBIDItreat, Martiensried, Germany) and transiently transfected with Lipofectamine2000 transfection reagent (Invivogen, Toulouse, France). 24h post transfection, nuclei were stained with Hoechst33342 (Sigma-Aldrich, Taufkirchen, Germany) and images were recorded using an ApoTome Imaging System, AxioVert Observer Z1 (YFP: Filter Set 46, DAPI: Filter Set 49, ApoTome, 63x/1.40 oil objective, ZEISS, Jena, Germany) in a quasi-confocal setting. The data demonstrate that all the mutants are expressed at similar, and wild-type-like, level in COS-7 cells (Extended Data Fig. 2).

### Quantification of receptor surface expression in COS-7 cells

COS-7 cells were seeded into black 96 well plates (Greiner, Kremsmünster, Austria), and transiently transfected with plasmid encoding receptor-eYFP fusion protein using MetafectenePro. 24h post transfection, cells were washed once with HBSS, and fluorescence was quantified using a plate reader (Tecan Infinite M200, Tecan, Männedorf, Switzerland) at excitation 488/5 nm and emission 530/5 nm. Data were normalized to mock transfected (0%) and wild type $Y_1R$-eYFP (100%), respectively. Results represent means ± s.e.m. from three independent experiments performed in quadruplicate.

### Peptide Synthesis

Porcine NPY (YPSKPDNPGEDAPAEDLARYYSALRHYINLITRQRY-$NH_2$) and NPY analogues were synthesized by automated solid-phase peptide synthesis (SPPS) on an automated multiple peptide synthesis robot system (Syro, MultiSynTech, Bochum, Germany), using a 9-fluorenylmethoxycarbonyl-*tert*-butyl (Fmoc/*t*Bu) strategy in 15 μM scale as previously described[43]. NPY-tyramide was synthesized as previously described[44]. Isotopically labelled NPY variants were prepared as described[16], and $^{13}C/^{15}N$ labelled amino acids were coupled manually with 2 eq. HOBT/DIC in DMF over night. The porcine variant of NPY, which contains a single mutation at position 17 from a methionine to leucine, was used, as this variant has identical binding affinity and signalling properties as human NPY with an increased solubility to assist in handling and will therefore be referred to as wild-type NPY[45].

Modified NPY analogues [$Bpa^1$,$K^4$[$(Ahx)_2$-biotin]]NPY and [$K^4$[$(Ahx)_2$-biotin]]NPY were synthesized by automated solid phase peptide synthesis and Bpa/Ahx/biotin were coupled manually using orthogonal Dde protection groups, cleaved by freshly prepared 3% (v/v) hydrazine in DMF for 10 × 5 min. Manual coupling reactions were performed by incubation of the resin with 5 eq. of the respective amino acid, 5 eq. HOBt and 5 eq. DIC in DMF for 2 h.

For biotin labelling, 3 eq. biotin was dissolved in DMF for 10 min at 60 °C. Next, 3 eq. HOBt and 3 eq. DIC were added to the mixture. Coupling was performed overnight at room temperature under constant shaking. Bpa containing peptides were cleaved from the resin and completely deprotected with a mixture of trifluoroacetic acid (TFA)/thioanisole (TA)/water (90:5:5 v/v/v).

All peptides were purified by preparative reversed-phase high-performance liquid chromatography (RP-HPLC) on a Jupiter 4u Proteo RP-C18 column (90 Å, 4 μm, Phenomenex), Kinetex 5u XB-C18 column (100 Å, 5 μm, Phenomenex), Kinetex 5u Biphenyl (100 Å, 5 μm, Phenomenex), Aeris 3.6 μm WIDEPORE XB-C18 (200 Å, 3.6 μm, Phenomenex) or Varitide RPC (200 Å, 6 μm, Agilent Technologies). All peptides were characterized by MALDI-ToF (Ultraflex III MALDI-ToF/ToF, Bruker daltonics) and ESI-HCT (High-capacity ion trap ESI-MS, Bruker Daltonics). Peptide purities were determined by two different analytical RP-HPLC systems and using 0.1% (v/v) TFA in $H_2O$ (eluant A) and 0.08% (v/v) TFA in acetonitrile (ACN) (eluant B). Purity of all peptides was ≥ 95%.

### NMR measurements of $Y_1$R-bound NPY

Fourteen differently isotopically labelled (U-$^{13}$C/$^{15}$N) porcine NPY peptides were prepared by standard Fmoc solid phase synthesis as described previously[16]. On the basis of the structure of micelle-bound NPY, the positions of the NMR labels were chosen to avoid signal overlap in $^{13}$C-$^{13}$C single quantum/double quantum correlation experiments and to allow straightforward signal assignment.

Expression of the human $Y_1$R in *E. coli* as inclusion bodies, inclusion body preparation, solubilization of the receptor in SDS and receptor purification was performed according to Schmidt *et al.*[46] yielding ~40-50 mg $Y_1$R per liter expression medium. To assemble the $Y_1$R into a functional state, a three step folding protocol was applied. In step 1, the purified $Y_1$ receptor was dialyzed against a degassed buffer containing 2 mM SDS, 50 mM NaP, pH 8.5, 1 mM EDTA, 1 mM reduced glutathione, and 0.5 mM oxidized glutathione at room temperature for 48 h. Subsequently, 25% (w/w) poly(ethylene glycol) (M.W. 20 kDa) was added to the buffer to concentrate the receptor before reconstitution. In step 2, bicelles consisting of 1,2-dimyristoyl-*sn*-glycero-3-phosphocholine (DMPC) / 1,2-diheptanoyl-*sn*-glycero-3-phosphocholine (DHPC-c7) (AvantiPolarLipids, Alabaster, USA) with a q value of 0.25 in 50 mM NaP, pH 8.0 were incubated with $Y_1$R, followed by three cycles of fast temperature cycles from 42°C to 0°C. Aggregated protein was removed instantly by centrifugation. In step 3, the $Y_1$R samples were concentrated in large bicelles (q > 20), which were used instead of liposomes because the high achievable receptor packing[46]. In large bicelles, all receptor binding sites are fully accessible. Subsequently, 50 mg ml$^{-1}$ BioBeadsSM2 was added at least twice to the solution. After removal of the beads with a sieve, samples were washed four times through cycles of pelleting by centrifugation and resolubilization in 50 mM NaP, pH 7.0. Concentration determination of the membrane embedded receptor was performed by solubilization of the bicelles in 10 times the volume of 15 mM SDS and 50 mM NaP, pH 7.0 and subsequent measurement of the $Y_1$R intrinsic absorption at 280 nm using UV-Vis. Labelled NPY variants in a slight molar excess were added to the $Y_1$R after detergent removal but before concentrating.

Assessment of the binding affinity of the $Y_1$R was carried out using homogenous fluorescence assays as described in the literature[47]. The reconstituted receptor was incubated in increasing concentrations with 50 nM fluorescently labelled NPY (NPY-atto520) overnight at room temperature in 50 mM NaP, pH 7.0 and 0.1% BSA. The fluorescence spectra were recorded on a FluoroMax-2 (JOBIN YVON) in a 10 mm quartz cuvette at

20 °C. The maximum signals of each spectrum were determined, normalized and plotted against the receptor concentration. The inflection point for $Y_1R$ binding was determined (OriginPro 8G / DoseResp) at $EC_{50}$ = 52 nM, demonstrating high functionality of the system. As a control, we used empty bicelles in concentrations, according to the bicelles concentration of the receptor samples, resulting in a lower binding ability to the ligand in comparison to the $Y_1R$.

NMR spectra were recorded on a Bruker Avance III 600 NMR spectrometer. The $^{13}C$ cross-polarization magic angle spinning (CP MAS) NMR experiments (0.7 ms contact time) were carried out using a double-resonance MAS probe with a 4 mm spinning module. Typical 90° pulse lengths were 4 μs for $^{1}H$ and $^{13}C$ and heteronuclear decoupling (SPINAL64) at a field strength of ~65 kHz. The $^{13}C$ chemical shifts were referenced relative to tetramethylsilane. The experiments were conducted at −30 °C and an MAS frequency of 7 kHz. The $^{13}C$ double quantum $^{13}C$ single quantum correlation spectra were acquired using the SPC-5 recoupling sequence[48] for double quantum excitation and reconversion (set to 0.571 ms each). The relaxation delay was 2.4 s.

## Molecular docking of NPY into $Y_1R$

Peptide docking of full-length porcine NPY was completed using Rosetta's FlexPepDock application[49]. Briefly, low energy backbone conformations were generated from the starting conformation of UR-MK299-bound $Y_1R$. Initially, the trimer of C-terminal NPY was docked into these conformations using full flexible docking guided by mutagenesis data. For each round of docking 5,000 models were generated. The models were sorted by total energy and binding energy. Top models from a given docking round were used to seed the next round of docking in which the peptide was extended. Fragment picking was performed using the fragment_picker application within Rosetta[26]. Secondary structure during fragment picking was guided by the NMR chemical shift data. Additionally, experimentally derived restraints were used to guide docking (R35-D287$^{6.59}$, R35-N283$^{6.55}$, Y36-Y100$^{2.64}$, R33-N299$^{7.32}$, L30-I293$^{ECL3}$). After docking peptides of length 6, 12, 18, and 36, the binding pocket was resampled to allow the ligand binding pocket to adopt to the shape of the peptide. This was accomplished with RosettaCM[50]. The $Y_1R$ crystal structure was used as a template along with the docked model to ensure the models did not drift too far from the starting structure though the N terminus was removed until the last docking step to provide steric bulk. Following full-length NPY docking, the N terminus of NPY was localized using loose distance constraints with the peptides identified in crosslinking experiments. Model selection from RosettaCM was accomplished using clustering to ensure backbone diversity. Following the identification of docked poses that satisfied the majority of experimental data, the chemical shifts of docked NPY peptides were calculated and filtered against the experimental NMR data to generate a final ensemble of docked poses with a 1.4 ppm root mean square distance to the experimental data. To analyse the binding interactions, per residue energetic analysis was calculated using the residue_energy_breakdown algorithm. The model with the lowest energy was selected as the representative binding pose (Fig. 4a). The ensemble is rather tight and therefore the individual binding poses are overall similar in structure (Fig. 4b).

### Photo-crosslinking experiment between $Y_1R$ and NPY N terminus

Cell-free expressed $Y_1R$ was produced by coupled in vitro transcription/translation based on the protocol from Schwarz *et al.*[51] using a bacterial cell lysate (S30 extract) from *E.coli* BL21 (DE3). Soluble membrane protein expression was achieved by addition of 0.1% (w/v) Brij-58, 1 mM GSSG and 5 mM GSH. Expression buffer was then exchanged to a binding buffer (0.1 M Tris/HCl, pH 7.4, 5% glycerol and 0.1% (w/v) Brij-58) and samples were purified by ligand affinity chromatography using [$K^4$[$(Ahx)_2$-biotin]]-NPY immobilized on Pierce Avidin Agarose beads (obtained from Thermo Fisher Scientific, Braunschweig, Germany) as previously described[52]. Elution was performed using 60 mM $CaCl_2$.

For photo-crosslinking $Y_1R$ in binding buffer was incubated with [$Bpa^1$,$K^4$[$(Ahx)_2$-biotin]]-NPY in a molar ratio of 4:1 (5 nmol:1.25 nmol) for 30 min at room temperature. In addition, the same reaction was performed with an 8 fold-excess of NPY ($Y_1R$:[$Bpa^1$,$K^4$[$(Ahx)_2$-biotin]]-NPY:NPY, 4:1:8). Subsequently, the opened reaction vessels were placed on ice and irradiated with UV light (UV lamp: Atkas Fluorest forte, λ = 366 nm, 180 W) for 90 min. 50 µl of photo-crosslinked $Y_1R$ sample (~ 200 µg) was digested with Glu-C and rLys-C (obtained from Promega, Mannheim, Germany) according to the manufacturer's protocol. Following, crosslinked fragments were isolated by affinity purification using Monomeric Avidin Agarose beads (obtained from Thermo Fisher Scientific, Braunschweig, Germany) according to the manufacturer's protocol. Possible fragments of digested $Y_1R$ were calculated by the online tool PeptideMass[53]. To mind incomplete digestion the tool was allowed for a maximum of five missed cleavages. For the analysis the combined option "Glu C (phosphate) + Lys-C" was chosen. Same was done for the calculation of possible NPY fragments. Theoretical masses of fragments after enzymatic cleavage of photo-crosslinked $Y_1R$ – [$Bpa^1$,$K^4$[$(Ahx)_2$-biotin]]NPY were calculated by adding possible $Y_1R$ fragment masses to NPY fragment masses containing the N terminus. The masses of Bpa, two times Ahx and biotin reduced by water for formation of a peptide bond were added manually. Peptide fragments of photo-crosslinked $Y_1R$ were analyzed by matrix-assisted laser desorption ionization time of flight mass spectrometry (MALDI-TOF MS) using an Ultraflex III MALDI-TOF/TOF mass spectrometer (Bruker Daltonics, Billerica, MA, USA).

Functionality of cell-free expressed $Y_1R$ samples was verified by a homogenous binding assay based on fluorescence polarization. We used [Dpr22-atto520]NPY (hereafter: NPY-atto520) as fluorescence tracer (IP accumulation in transiently transfected COS-7: $EC_{50}$ = 24 nM, $pEC_{50}$ = −7.16 ± 0.20). 50 nM of NPY-atto520 was incubated with increasing concentrations of $Y_1R$ in Brij-58 micelles in buffer (0.1 M Tris/HCl, pH 7.4, 2.5% glycerol, 0.1% (w/v) Brij-58 and 0.1% bovine serum album) for 90 min under gentle agitation in opaque 96 well plates. Fluorescence was then measured in a Tecan Spark plate reader (Tecan, Männedorf, Switzerland) using linear polarized light, excitation 510/5 nm, emission 550/10 nm, 90° detection angle. Experiments were conducted at least twice independently in duplicate.

### Data availability

Atomic coordinates and structure factor files for the $Y_1R$–UR-MK299 and $Y_1R$–BMS-193885 complex structures have been deposited in the Protein Data Bank with identification codes 5ZBQ and 5ZBH, respectively.

## Extended Data

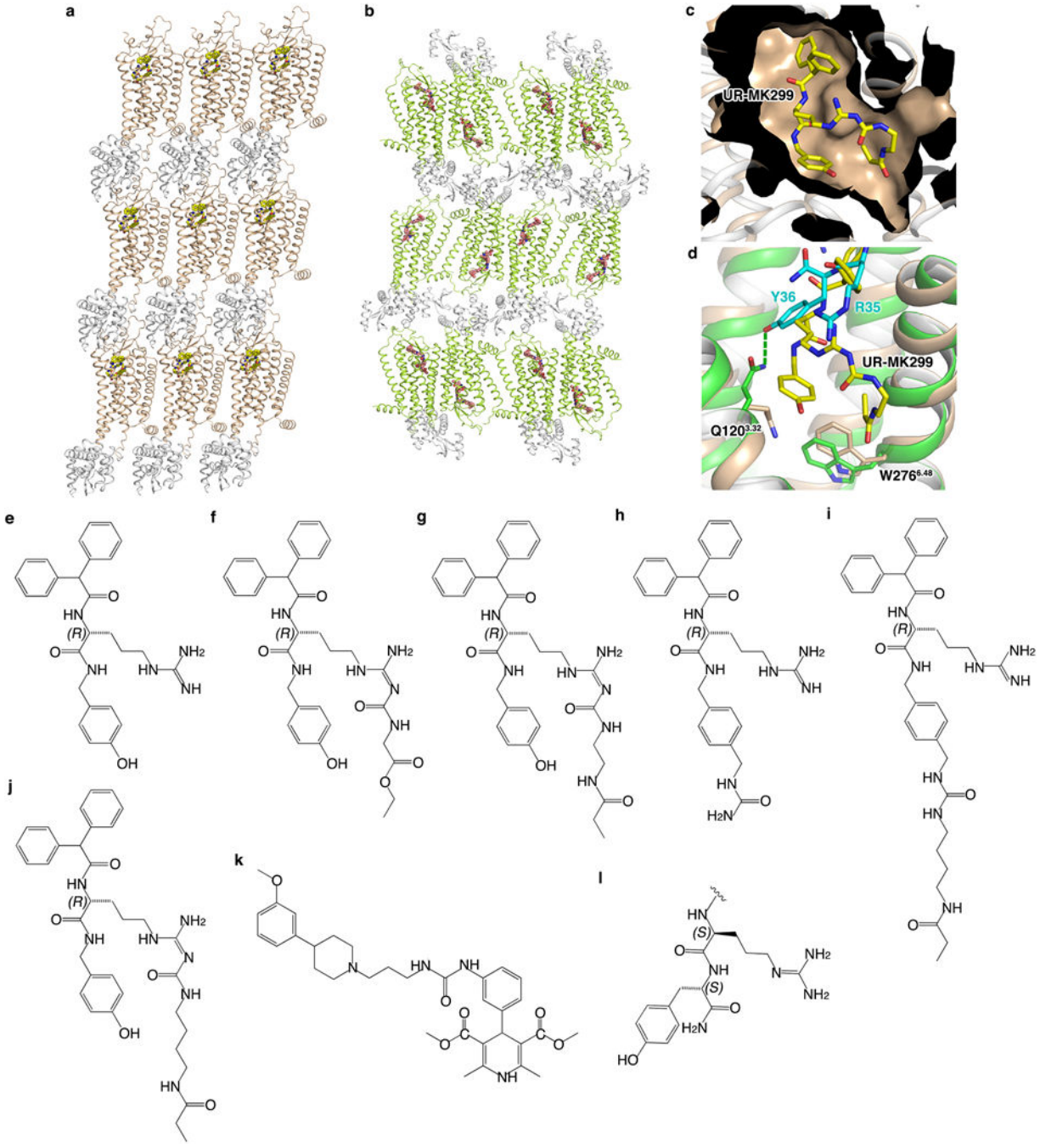


**Extended Data Figure 1. Crystal packing and structural features of $Y_1R$ and chemical structures of $Y_1R$ ligands**

**a, b**, Crystal packing of $Y_1R$–UR-MK299 (**a**) and $Y_1R$–BMS-193885 (**b**) complexes. $Y_1R$ is shown in cartoon representation and coloured brown and green in the $Y_1R$–UR-MK299 and $Y_1R$–BMS-193885 complexes, respectively. The T4L fusion is shown in grey cartoon representation. UR-MK299 and BMS-193885 are displayed as yellow and pink spheres, respectively. **c**, Cutaway view of UR-MK299 binding pocket in $Y_1R$. The receptor is shown in brown cartoon and surface representations. The ligand is shown as yellow sticks. **d**, Comparison of $Y_1R$ between the $Y_1R$–UR-MK299 crystal structure (brown) and $Y_1R$–NPY model (green). Side chains of $Q120^{3.32}$ and $W276^{6.48}$ are shown as sticks. R35-Y36 of NPY is displayed as cyan sticks. The hydrogen bond between $Q120^{3.32}$ and Y36 of NPY is shown as a green dashed line. **e**-**j**, Chemical structures of argininamide $Y_1R$ antagonists, BIBP3226 (**e**), UR-HU404 (**f**), UR-MK299 (**g**), BIBO3304 (**h**), UR-MK289 (**i**) and UR-MK136 (**j**). **k**, Chemical structure of BMS-193885. **l**, Scaffold of NPY C-terminal residues R35 and Y36. Key differences between R35-Y36 of NPY and UR-MK299 are chirality of the arginine derivative and alteration of bond connectivity leading to the hydroxyphenyl group.

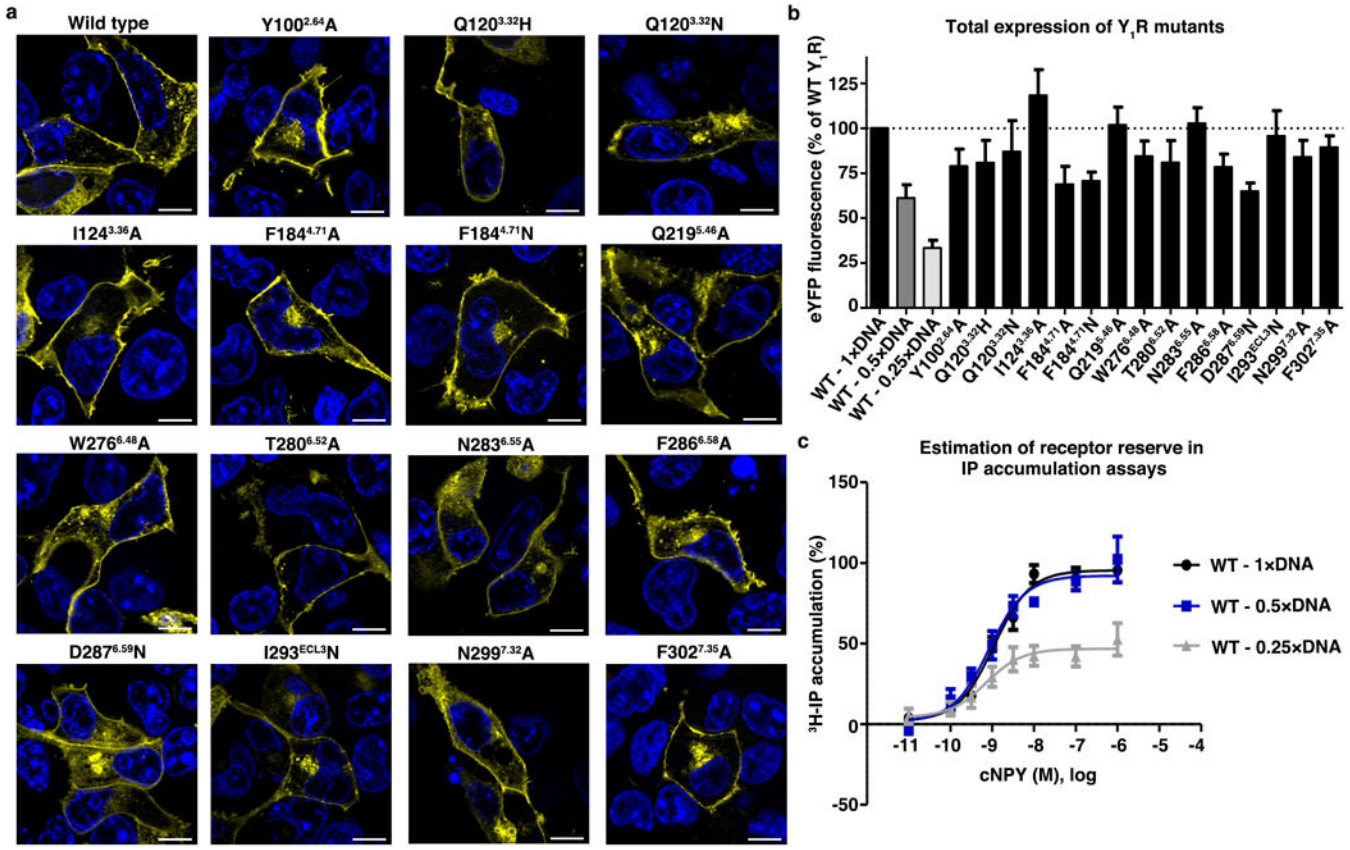


**Extended Data Figure 2. Expression of wild-type and mutant $Y_1$Rs in transiently transfected COS-7 cells**

**a**, Live cell fluorescence microscopy verifies all $Y_1R$ variants to be properly folded and exported to the cell membrane like the wild-type receptor. Nuclei stained with Hoechst33342, bar equals 10 μm. Pictures are representative of two independent experiments with similar results. **b**, Total expression level was determined by fluorescence reading and confirmed expression similar to the wild type. Transfection of only 50% or 25%

of the DNA amount (with total DNA amount held constant by empty vector), respectively, led to a proportial decrease of fluorescence, and thus, expression level. Data represent means ± s.e.m of three to five independent experiments performed in technical triplicate (see source data for sample size n of each mutant). **c**, Estimation of the receptor reserve in functional IP accumulation assays. Transfection of half of the vector encoding receptor (with constant total DNA amount including chimeric G protein, *cf.* a) still produces maximum signal, while further reduction results in signal loss at comparable potency. Thus, there is only a small receptor reserve in the functional readout, allowing potency alteration to be directly related to compromised ligand binding. Data represent means ± s.e.m of three independent experiments performed in technical duplicate.

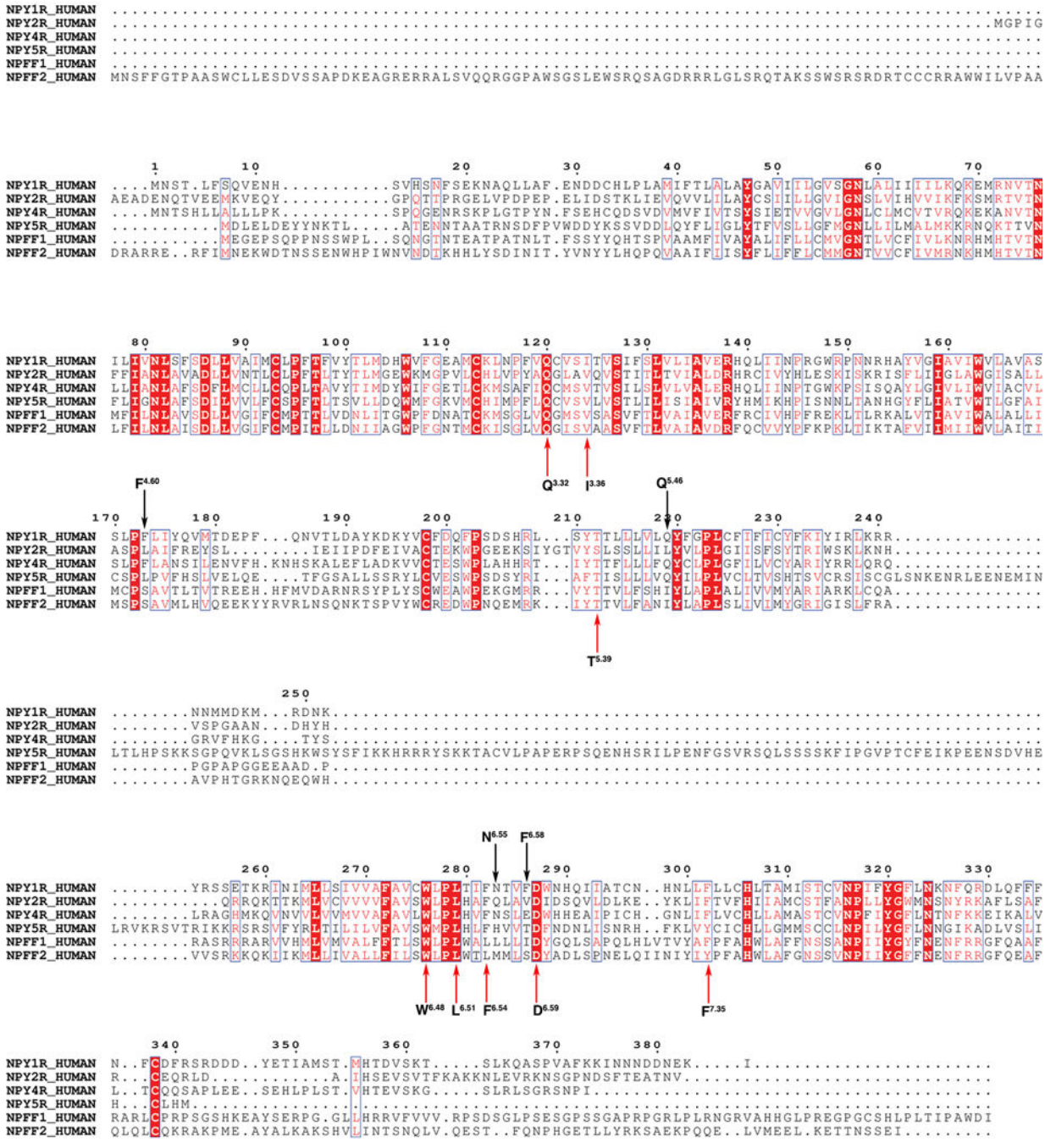


**Extended Data Figure 3. Sequence alignment of the human NPY receptors and the human NPFF receptors**

Colours represent similarities of residues: red background, identical; red, strongly similar. Key residues in the UR-MK299 binding pocket, which are conserved or variable among receptors, are indicated by red and black arrows, respectively. The alignment was generated by uniprot (http://www.uniprot.org/align/) and graphic was prepared on ESPript 3.0 server (http://espript.ibcp.fr/ESPript/cgi-bin/ESPript.cgi).

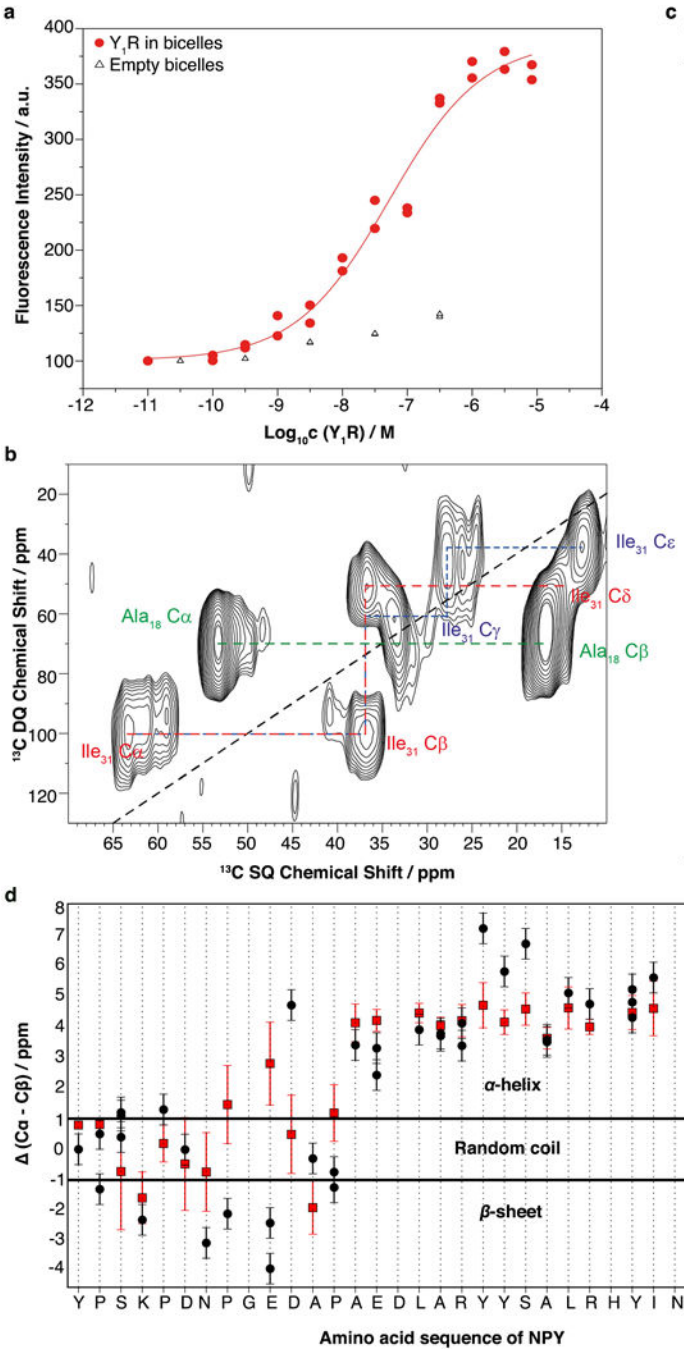


c

| | $C_\alpha$ | $C_\beta$ | $C_\gamma$ | $C_\delta$ | $C_\varepsilon$ |
|---|---|---|---|---|---|
| Y1 | 57.2 | 39.0 | | | |
| P2 | 62.0 | 31.7 | 24.6 | 48.0 | |
| S2 | 58.0 | 63.3 | | | |
| K4 | 53.1 | 32.3 | 25.1 | 28.8 | 41.0 |
| P5 | 62.1 | 30.1 | 27.0 | 48.5 | |
| D6 | 52.6 | 40.0 | | | |
| N7 | 48.0 | 37.0 | | | |
| P8 | 56.7 | 28.1 | 25.9 | 48.8 | |
| G9 | | | | | |
| E10 | 54.9 | 32.1 | 27.9 | | |
| D11 | 56.0 | 38.7 | | | |
| A12 | 48.5 | 16.0 | | | |
| P13 | 60.1 | 30.8 | 24.7 | 46.7 | |
| A14 | 53.3 | 17.1 | | | |
| E15 | 56.6 | 27.7 | 27.7 | | |
| L17 | 55.6 | 39.7 | 25.5 | 25.5 | 25.5 |
| A18 | 53.3 | 16.7 | | | |
| R19 | 57.8 | 29.2 | 24.7 | 41.5 | |
| Y20 | 60.5 | 35.1 | | | |
| Y21 | 60.3 | 36.3 | | | |
| S22 | 60.8 | 60.1 | | | |
| A23 | 52.9 | 16.6 | | | |
| L24 | 56.9 | 39.8 | 25.5 | 25.5 | 25.5 |
| R25 | 57.7 | 28.0 | 24.4 | 41.1 | |
| Y27 | 60.2 | 37.4 | | | |
| I28 | 63.5 | 36.2 | 28.1 | 16.6 | 12.4 |
| L30 | 56.5 | 39.8 | 25.8 | 25.8 | 25.8 |
| I31 | 63.0 | 36.7 | 27.4 | 16.8 | 12.7 |
| T32 | 60.2 | 65.4 | 18.0 | | |
| R33 | 54.3 | 29.1 | 23.7 | 42.7 | 54.3 |
| Q34 | 54.0 | 27.4 | 29.1 | | |
| R35 | 52.5 | 29.6 | 25.0 | 41.8 | |
| Y36 | 54.7 | 38.7 | | | |

**Extended Data Figure 4. Pharmacological characterization of refolded $Y_1R$ and NMR studies of $Y_1R$-bound NPY**

**a**, Binding of atto520-labelled NPY (50 nM) to increasing amounts of $Y_1R$-containing bicelles or empty bicelles. Data reflect fluorescence enhancement upon binding. An inflection point at $EC_{50}$ = 52 nM was determined. Two independent experiments were performed in technical duplicate with similar results. Data shown are from a representative experiment. **b**, Typical $^{13}C$ MAS single quantum (SQ) / double quantum (DQ) correlation spectrum of NPY in the presence of $Y_1R$ reconstituted into large bicelles at −30 °C. NMR

spectra were acquired from 1 to 3 independent preparations for each labelled amino acid with similar results (see panel d). Data shown are from a representative experiment. **c**, Table showing $^{13}C$ NMR chemical shifts of assigned amino acids of NPY bound to $Y_1R$ (referenced to tetramethylsilane) as acquired in solid-state NMR experiments. **d**, $^{13}C$ chemical-shift index of NPY bound to $Y_1R$ in large DMPC/DHPC-c7 bicelles (q > 20) compared with docked models. Plotted is the measured chemical shift difference (Cα-Cβ) for each individual residue of NPY subtracted by chemical shift difference of the same amino acid type in random coil conformation in black. Individual data points from 1 to 3 independent experiments for each labelled amino acid are shown. Typical experimental errors in determining chemical shifts under these conditions are ±1 ppm. Chemical shifts were back-calculated for the top docking solutions and filtered against the experimental data to generate a final ensemble of docked poses. Their average chemical-shift index and associated standard deviation from 10 top docked poses are shown in red.

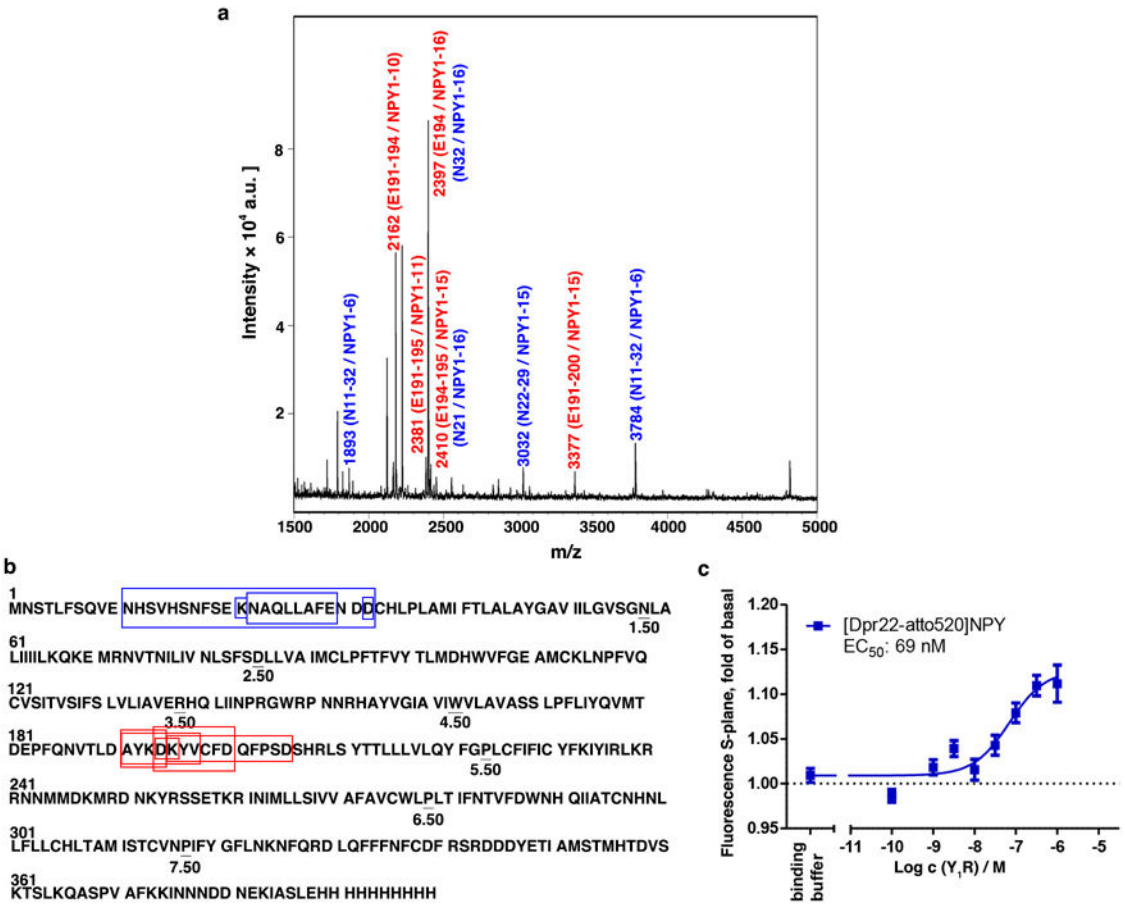


**Extended Data Figure 5. Photo-crosslinking experiments between NPY and $Y_1R$**

**a**, Mass spectra of photo-crosslinked $Y_1R$ with [$Bpa^1$,$K^4$[$(Ahx)_2$-biotin]]NPY. Exemplary MALDI-ToF mass spectra of photo-crosslinked samples enzymatically digested by rLys-C and Glu-C. Potential $Y_1R$ fragments are labelled. Two independent experiments were performed with similar results. N, N terminus of $Y_1R$ (blue); E, ECL2 (red). **b**, Respective regions of NPY N terminus at $Y_1R$. Amino acid sequence of $Y_1R$ with a C-terminal His-tag.

The two detected regions within $Y_1R$ (N terminus (blue), ECL2 (red)) after crosslinking with [$Bpa^1$,$K^4$[$(Ahx)_2$-biotin]]NPY are emphasized in boxes. The different sizes of the boxes represent different detected fragments (Extended Data Table 5), respectively. Experiments were repeated twice independently with similar results, and only fragements that were observed in both experiments are listed here and in Extended Data Table 5. **c**, Binding of atto520-labelled NPY (50 nM) to increasing amounts of cell-free produced $Y_1R$ in Brij-58. Data reflect fluorescence enhancement upon binding. $EC_{50}$ value of 69 nM was determined. Data shown are means ± s.e.m. from six independent experiments performed in technical triplicate.

## Extended Data Table 1

Data collection and refinement statistics

| | **$Y_1R$–UR-MK299** | **$Y_1R$–BMS-193885** |
|---|---|---|
| Data Collection* | | |
| Space group | *$P2_1$* | *$C222_1$* |
| Cell dimensions | | |
| a, *b, c* (Å) | 37.8, 100.7, 83.2 | 76.9, 126.8, 170.3 |
| α, β, γ (°) | 90.0, 98.8, 90.0 | 90.0, 90.0, 90.0 |
| Resolution (Å) | 50.0-2.7 (2.8-2.7)† | 50.0-3.0 (3.1-3.0) |
| $R_{merge}$ (%) | 23.7 (83.9) | 16.6 (93.7) |
| $I/\sigma I$ | 5.01 (0.71) | 5.30 (1.00) |
| Completeness (%) | 93.0 (87.0) | 92.4 (79.2) |
| Redundancy | 7.4 (2.3) | 3.5 (2.6) |
| **Refinement** | | |
| Resolution (Å) | 50.0-2.7 | 50.0-3.0 |
| No. reflections | 15,818 (758) | 15,600 (797) |
| $R_{work}/R_{free}$ (%) | 22.4/26.6 | 22.4/24.9 |
| Number of atoms | | |
| Protein | 3,791 | 3,654 |
| Ligand | 45 | 43 |
| Overall *B* values (Å$^2$) | | |
| Protein | 88.3 | 108.0 |
| Ligand | 66.4 | 81.0 |
| R.m.s. deviations | | |
| Bond lengths (Å) | 0.009 | 0.009 |
| Bond angles (°) | 1.01 | 1.00 |

*Diffraction data from 47 $Y_1R$–UR-MK299 crystals and 33 $Y_1R$–BMS-193885 crystals were used to solve the structures.

†Numbers in parentheses refer to the highest-resolution shell.

## Extended Data Table 2

IP accumulation assays of wild-type and mutant $Y_1$Rs for NPY and antagonists

| Mutants | NPY | | NPY/BIBP3226 ($10^{-5}$ M)* | | | | NPY/BIBO3304 ($10^{-6}$ M) | | | | NP |
|---|---|---|---|---|---|---|---|---|---|---|---|
| | $EC_{50}$ (nM)† ($pEC_{50}$ ± SEM) | n‡ | $EC_{50}$ (nM) ($pEC_{50}$ ± SEM) | Ratio§ | $K_b$(nM)// | n | $EC_{50}$ (nM) ($pEC_{50}$ ± SEM) | Ratio | $K_b$(nM) | n | $EC_{50}$ (nM) ($pEC_{50}$ ± SEM) |
| Wild type | 1.7 (8.78 ± 0.03) | 20 | 463 (6.43 ±0.04) | 272 | 36.9 | 14 | 175 (6.76 ± 0.04) | 103 | 9.8 | 16 | 1,099/126# (5.96 ± 0.04)/(6.90 ± 0.07) |
| Y100$^{2.64}$A | 562;404 | 2 | nd | nd | nd | 2 | nd | nd | nd | 2 | nd |
| Q120$^{3.32}$H | 12; 15 | 2 | nd | nd | nd | 2 | nd | nd | nd | 2 | >50,000; >50,000 |
| Q120$^{3.32}$N | 3.8 (8.42 ± 0.07) | 4 | 836 (6.08 ± 0.06) | 220 | 45.7 | 3 | 414 (6.38 ± 0.09) | 109 | 9.3 | 3 | 3,744 (5.43 ± 0.10) |
| I124$^{3.36}$A | 6.0 (8.22 ± 0.08) | 3 | 1,877 (5.73 ± 0.06) | 313 | 32.1 | 4 | 306 (6.52 ± 0.06) | 51 | 20.0 | 4 | 1,588 (5.80 ± 0.06) |
| Q219$^{5.46}$A | 23 (7.63 ± 0.05) | 7 | 2,732 (5.56 ± 0.08) | 119 | 84.8 | 4 | 1,156 (5.94 ± 0.07) | 50 | 20.4 | 3 | >10,000/1,711#; 2,197 |
| W276$^{6.48}$A | 3.8 (8.42 ± 0.06) | 5 | 246 (6.61 ± 0.12) | 65 | 156 | 3 | 84; 60 | 22; 16 | 47; 68 | 2 | 490; 254 |
| T280$^{6.52}$A | 2.6 (8.58 ± 0.08) | 4 | 141 (6.85 ± 0.08) | 54 | 189 | 4 | 124 (6.91 ± 0.05) | 48 | 21.3 | 4 | 871 (6.06 ± 0.08) |
| N283$^{6.55}$A | 900 (6.05 ± 0.06) | 7 | 1,148 (5.94 ± 0.12) | 1 | nd | 3 | 1,036 (5.98 ±0.14) | 1 | nd | 3 | 7,622 (5.12 ± 0.14) |
| F286$^{6.58}$A | 4.5 (8.35 ± 0.04) | 7 | 491 (6.31 ± 0.05) | 109 | 92.6 | 3 | 118 (6.93 ± 0.09) | 26 | 40.0 | 3 | 1,553 (5.81 ± 0.05) |
| D287$^{6.59}$N | 260 (6.59 ± 0.05) | 7 | 900; 748 | 3.5; 2.9 | 4065; 5328 | 2 | 341; 142 | 1 | nd | 2 | >20,000; 1,571# (5.80 ± 0.12) |
| F302$^{7.35}$A | 4.2 (8.38 ± 0.09) | 3 | 16; 29 | 4; 7 | 3,570; 1,695 | 2 | 4.4; 10.1 | 1; 2.4 | nd; 712 | 2 | 33; 42 |

*Antagonist concentrations were chosen based on their antagonistic activity on $Y_1$R.

†$EC_{50}$ values were determined after 1 h stimulation by increasing concentration of NPY or NPY together with different antagonists. Data are shown as means from at least three independent experiments (n>2) or results of two individual experiments (n=2) each performed in technical duplicate.

‡Sample size n, the number of independent experiments performed in technical duplicate.

§The $EC_{50}$ ratio represents the shift between the NPY and NPY/antagonist curve ($EC_{50(NPY+antagonist)}$ / $EC_{50(NPY)}$) and characterizes the antagonistic effect on wild-type receptor or receptor mutants. By comparison of $EC_{50}$ ratios between wild type and receptor mutant, influences of all tested residues on antagonist activity were determined. The higher ratio, the higher antagonist activity. A reduced $EC_{50}$ ratio of mutant compared to the wild-type receptor was interpreted as important for the respective antagonist.

//$K_b$ values were determined using the Gaddum transformation ($K_b$ = [Antagonist] / ($EC_{50}$ ratio – 1)).

#These data were obtained at a reduced concentration of UR-HU404 ($10^{-8}$ M) as concentration response curves did not reach saturation ($EC_{50}$ > 10,000 nM) when high concentration was used ($10^{-7}$ M).

nd: not determined; /: not tested.

## Extended Data Table 3

Binding of $Y_1R$ antagonists and agonists to membrane preparations from *Sf*9 cells expressing wild-type and mutant $Y_1Rs$

**a. Binding of antagonists to wild-type and mutant $Y_1Rs$**

| $Y_1R$ mutants | $K_d$ (nM)* | | $K_i$ (nM)† | | | | | | | | | |
|---|---|---|---|---|---|---|---|---|---|---|---|---|
| | [$^3$H]-UR-MK299 | n‡ | BMS-193885 | n | BIBP3226 | n | BIBO3304 | n | UR-MK136 | n | UR-MK289 | n |
| Wild type | 0.17 ± 0.03 | 3 | 22 ± 6 | 3 | 2.4; 3.1 | 2 | 1.6 ± 0.3 | 3 | 2.8; 4.0 | 2 | 25; 28 | 2 |
| Crystallization construct | 0.33 ± 0.06 | 3 | 38 ± 2 | 4 | / | | / | | / | | / | |
| C121$^{3.33}$A | 1.4; 2.4 | 2 | / | | / | | / | | / | | / | |
| I124$^{3.36}$A | 7.0; 8.0 | 2 | 9,500 ± 1,700 | 3 | 15 ± 5 | 3 | 11 ± 2 | 3 | 12 ± 2 | 3 | 80 ± 16 | 3 |
| I124$^{3.36}$F | 1.3; 1.9 | 2 | / | | / | | / | | / | | / | |
| F173$^{4.60}$A | 9.1 ± 2.2 | 4 | 590 ± 220 | 3 | 68; 84 | 2 | 120 ± 17 | 4 | 88; 110 | 2 | 660 ± 110§ | 5 |
| F173$^{4.60}$W | 0.31; 0.32 | 2 | 110; 130 | 2 | 15; 26 | 2 | 13 ± 4 | 3 | 3.6; 4.3 | 2 | 6.8; 9.2 | 2 |
| T212$^{5.39}$A | 0.12; 0.18 | 2 | 150; 150 | 2 | 13; 12 | 2 | 2.5 ± 0.3 | 3 | 5.7; 7.5 | 2 | 18; 21 | 2 |
| L215$^{5.42}$G | 4.2; 5.6 | 2 | 9.6 ± 1.9 | 4 | 43; 23 | 2 | 47 ± 4 | 3 | 11; 8.4 | 2 | 29; 30 | 2 |
| Q219$^{5.46}$A | 4.1; 5.1 | 2 | 0.50 ± 0.07 | 4 | 35; 53 | 2 | 6.2 ± 0.7 | 3 | 16 ± 4 | 3 | 13 ± 4 | 3 |
| Q219$^{5.46}$V | 5.1 ± 1.2 | 3 | / | | / | | / | | / | | / | |
| W276$^{6.48}$A | >500 | 3 | / | | / | | / | | / | | / | |
| L279$^{6.51}$A | 1.0; 1.1 | 2 | 160; 220 | 2 | 110; 110 | 2 | 13 ± 2 | 3 | 120; 150 | 2 | 320 ± 40 | 3 |
| T280$^{6.52}$A | 0.16 ± 0.04 | 3 | 7,300 ± 1,300 | 3 | 32 ± 7 | 3 | 2.6 ± 0.4 | 3 | 4.2 ± 1.1 | 3 | 8.2 ± 4.2 | 3 |
| N283$^{6.55}$A | >500; >500 | 2 | / | | / | | / | | / | | / | |
| D287$^{6.59}$A | >500; >500 | 2 | / | | / | | / | | / | | / | |
| F302$^{7.35}$A | >500; >500 | 2 | / | | / | | / | | / | | / | |

**b. Binding of NPYs to wild-type $Y_1R$**

| | $K_d$ (nM)* | | $K_i$ (nM)† | | | |
|---|---|---|---|---|---|---|
| $Y_1R$ | [$^3$H]-UR-MK299 | n | Human NPY | n | Porcine NPY | n |
| Wild type | 0.89; 1.1 | 2 | 4.1; 4.2 | 2 | 2.8 ± 0.4 | 4 |

*Dissociation constant determined by saturation binding at *Sf*9 membranes (receptor expression was confirmed by western blot analysis) using a sodium-containing buffer (a) or a sodium-free buffer (b) (Note: the sodium-free buffer was used for the determination of agonist binding affinity because porcine NPY exhibited approx. 10-fold higher affinity in the sodium-free buffer compared to the sodium-containing buffer (data not shown)).

†Dissociation constant determined by competition binding with [$^3$H]-UR-MK299 at *Sf*9 membranes using a sodium-containing buffer (a) or a sodium-free buffer (b).

‡Sample size, the number of independent experiments performed in technical triplicate. If n>2, data are shown as means ± s.e.m. If n=2, results of two individual experiments are shown.

§The lower curve plateau of the four-parameter logistic fit, amounting to 17±3% of specifically bound [$^3$H]-UR-MK299 (mean ± s.e.m. from five independent experiments), was different from zero ($P < 0.005$, one-sample one-tailed t-test), which is indicative of a non-competitive mechanism.

/: not tested.

## Extended Data Table 4

IP accumulation assays of wild-type (WT) and mutant $Y_1$Rs for NPY/NPY analogues

**a. IP accumulation assays of complementary mutagenesis between NPY/NPY analogues and WT and mutant $Y_1$Rs**

| | WT | | | Q 120$^{3.32}$H | | | I293$^{ECL3}$N | | | N |
|---|---|---|---|---|---|---|---|---|---|---|
| **Peptides*** | **$EC_{50}$ (nM)† ($pEC_{50}$ ± SEM)** | **X-fold over WT‡** | **n§** | **$EC_{50}$ (nM) ($PEC_{50}$ ± SEM)** | **X-fold over WT** | **n** | **$EC_{50}$ (nM) ($PEC_{50}$ ± SEM)** | **X-fold over WT** | **n** | **E (** |
| **NPY** | 1.5 (8.83 ± 0.02) | 1 | 51 | 39 (7.41 ±0.11) | 26 | 3 | 169 (6.77 ± 0.08) | 113 | 8 | 91 ( |
| **[N$^{30}$]NPY** | 289 (6.54 ± 0.06) | 1 | 9 | *1* | / | / | 3116; 1274 | 11; 4 | 2 | |
| **[A$^{33}$]NPY** | 5,395 (5.27 ± 0.07) | 1 | 3 | / | / | / | / | / | / | 5, |
| **[A$^{35}$]NPY** | >10,000 | 1 | 3 | / | / | / | / | / | / | |
| **[A$^{36}$]NPY** | 1,378 (5.86 ± 0.06) | 1 | 6 | / | / | / | / | / | *i* | |
| **NPY-tyramide** | 68 (7.17 ±0.11) | 1 | 9 | nd | nd | 3 | / | *i* | *i* | |

**b. IP accumulation assays of WT $Y_1$R for NPY/NPY analogues**

| | **NPY** | **Ac-NPY** | **[A$^1$]NPY** | **[A$^2$]NPY** | **[A$^1$,A$^2$]NPY** | **NPY(3-36)** | **NPY(13-36)** |
|---|---|---|---|---|---|---|---|
| **$EC_{50}$ (nM) ($pEC_{50}$ ± SEM)** | 1.5 (8.83 ± 0.02) | 0.5; 3.0 | 6.5; 2.4 | 7.3 (8.14 ±0.11) | 8.0 (8.10 ±0.06) | 83 (7.08 ± 0.09) | 477;744 |
| **X-fold over NPY** | 1 | 1; 2 | 4; 2 | 5 | 5 | 55 | 318; 496 |
| **n** | 51 | 2 | 2 | 4 | 3 | 3 | 2 |

**c. NPY-induced IP accumulation assays of WT and mutant $Y_1$Rs**

| | **WT** | **F184$^{ECL2}$A** | **F184$^{ECL2}$N** | **V187$^{ECL2}$N** | **L189$^{ECL2}$N** | **Y192$^{ECL2}$S** | **V197$^{ECL2}$A** | **V197$^{ECL2}$N** | **F199$^{ECL2}$N** |
|---|---|---|---|---|---|---|---|---|---|
| **$EC_{50}$ (nM) ($pEC_{50}$ ± SEM)** | 1.5 (8.83 ± 0.02) | 18.7 (7.73 ± 0.08) | 23 (7.64 ±0.10) | 1.9 (8.72 ± 0.08) | 1.9 (8.73 ± 0.16) | 3.8 (8.42 ± 0.11) | 1.9 (8.71 ± 0.13) | 188 (6.73 ± 0.11) | 3.4 (8.47 ± 0.11) |
| **X-fold over WT** | 1 | 13 | 15 | 1 | 1 | 2.5 | 1 | 125 | 2 |
| **n** | 51 | 7 | 14 | 3 | 3 | 3 | 5 | 7 | 3 |

*Peptides were synthesized following the methods described in peptide synthesis section of Methods.

†$EC_{50}$ were determined using GraphPad Prism 5.0. All curves were normalized to the top and bottom values of the $Y_1$R/NPY curve. Nonlinear regression (curve fit) was performed for normalized response in all assays. All data are shown as means from at least three independent experiments (n>2) or results of two individual experiments (n=2) each performed in technical duplicate.

‡The $EC_{50}$ shifts were determined by $EC_{50(mutant)}$ / $EC_{50(WT)}$, set Hill slope to 1. For the wild-type receptor x-fold is set to 1. Lower $EC_{50}$ shift of NPY analogue/mutant compared to NPY/mutant was interpreted as no further loss of function and a direct interaction between both positions.

§Sample size n, the number of independent experiments performed in technical duplicate.

//Data are from reference 27.

nd, not determined up to $10^{-4}$ M agonist concentration; /, not tested.

## Extended Data Table 5

Mass spectromeric signals and calculated mass of photo-crosslinked $Y_1R$ with [Bpa[1],K[4][(Ahx)$_2$-biotin]]NPY

| MALDIToF MS (m/z)* | Number in $Y_1R$ | Position [Bpa[1],K[4][(Ahx)$_2$-biotin]]NPY | $M_{calc.}$(Da)† | [$M_{calc}$ + (Da) | [$M_{calc}$ + Na]$^+$(Da) | [$M_{ca}$ + K] (Da |
|---|---|---|---|---|---|---|
| 1824.2 | | | not identified | | | |
| 1867.3 | | | not identified | | | |
| 1892.6 | 11–32 | 1 – 6 | 3760.7 | 3761.8 | 3783.7 | 3799 |
| 1988.2 | – | 1–11 + 5–6 | 1986.9 | 1987.9 | 2009.9 | 2025 |
| 2001.1 | – | 1–10 + 5–7 | 2000.0 | 2001.0 | 2022.9 | 2038 |
| 2059.2 | – | 1–10 + 8–11 | 2057.9 | 2058.9 | 2080.9 | 2096 |
| | – | 1–11 +8–10 | 2057.9 | 2058.9 | 2080.9 | 2096 |
| 2073.2 | | | not identified | | | |
| | – | 1–10 + 8–11 | 2057.9 | 2058.9 | 2080.9 | 2096 |
| 2081.3 | – | 1–11 +8–10 | 2057.9 | 2058.9 | 2080.9 | 2096 |
| 2121.3 | | | not identified | | | |
| 2162.2 | 191 – 194 | 1 – 10 | 2139.0 | 2140.0 | 2162.0 | 2178 |
| 2311.4 | | | not identified | | | |
| 2317.4 | | | not identified | | | |
| 2381.4 | 191 – 195 | 1–11 | 2380.1 | 2381.1 | 2403.1 | 2419 |
| 2381.8 | 195–205 | 1 – 4 | 2381.1 | 2382.1 | 2404.1 | 2420 |
| 2397.3 | 32–32 | 1 – 16 | 2374.0 | 2375.0 | 2397.0 | 2413 |
| | 194–194 | 1 – 16 | 2374.0 | 2375.0 | 2397.0 | 2413 |
| | 21 – 21 | 1 – 16 | 2387.1 | 2388.1 | 2410.1 | 2426 |
| 2410.3 | 195 – 195 | 1 – 16 | 2387.1 | 2388.1 | 2410.1 | 2426 |
| | 194–195 | 1 – 15 | 2387.1 | 2388.1 | 2410.1 | 2426 |
| 2413.3 | 32–32 | 1 – 16 | 2374.0 | 2375.0 | 2397.0 | 2413 |
| | 194 – 194 | 1 – 16 | 2374.0 | 2375.0 | 2397.0 | 2413 |
| 2450.4 | – | 1–15 + 8–10 | 2427.1 | 2428.1 | 2450.1 | 2466 |
| 2514.5 | | | not identified | | | |
| 2553.5 | 194 – 200 | 1 – 10 | 2530.1 | 2531.1 | 2553.1 | 2569 |
| 2589.6 | | | not identified | | | |
| 2775.7 | | | not identified | | | |
| 2807.7 | | | not identified | | | |
| 3031.7 | 22–29 | 1 – 15 | 3030.4 | 3031.4 | 3053.4 | 3069 |
| 3377.7 | 191 – 200 | 1 – 15 | 3376.5 | 3377.5 | 3399.5 | 3415 |
| 3784.1 | 11–32 | 1 – 6 | 3760.7 | 3761.8 | 3783.7 | 3799 |
| 3966.3 | – | 1–7 + 17–36 | 3943.1 | 3944.1 | 3966.1 | 3982 |
| 4524.9 | | | not identified | | | |

*Determined signals by MALDI-ToF MS.

†Selected calculated masses in Dalton of possible photo-crosslinked fragments of $Y_1R$ with [Bpa[1],K[4][(Ahx)$_2$-biotin]]NPY or [Bpa[1],K[4][(Ahx)$_2$-biotin]]NPY with itself. The fragments are selected based on the correlation with the detected signals. For clarity, further calculated masses of possible photo-crosslinked fragments are not shown.

## Acknowledgments

This work was supported by CAS Strategic Priority Research Program XDB08020000 (B.W.), the Key Research Program of Frontier Sciences, CAS, Grant no. QYZDB-SSW-SMC024 (B.W.) and QYZDB-SSW-SMC054 (Q.Z.), the National Science Foundation of China grants 31570739 (B.W.), 81525024 (Q.Z.) and 3170040264 (Z.Y.), the European Community, the Free State of Saxony (SAB 100148835 to D.H. and 100881433 to A.G.B.-S.) and the Deutsche Forschungsgemeinschaft (DFG) (Be1264-16, SFB 1052/A3, research grant KE 1857/1-1 and Graduate Training Program GRK 1910). Work in the Meiler laboratory is supported through NIH (R01 GM080403, R01 DK097376, R01 HL122010) and NSF (CHE 1305874). T. Zellmann for his contribution to the modelling in the early state of the project and the technical support of R. Reppich-Sacher (mass spectrometry) and K. Löbner (cell culture) are kindly acknowledged. The authors thank Dr. H. A. Scheidt for support with ssNMR measurements and M. Beer-Krön, D. Fritsch, S. Bollwein and B. Wenzl for expert help in performing radioligand binding experiments. The synchrotron radiation experiments were performed at the BL41XU of SPring-8 with approval of the Japan Synchrotron Radiation Research Institute (proposal no. 2015B2026, 2015B2027, 2016A2517, 2016A2518, 2016B2517 and 2016B2518). We thank the beamline staff members K. Hasegawa, H. Okumura, N. Mizuno, T. Kawamura and H. Murakami of the BL41XU for help on X-ray data collection.

## References

1. Zhang L, Bijker MS, Herzog H. The neuropeptide Y system: pathophysiological and therapeutic implications in obesity and cancer. Pharmacol Ther. 2011; 131:91–113. [PubMed: 21439311]
2. Morales-Medina JC, Dumont Y, Quirion R. A possible role of neuropeptide Y in depression and stress. Brain Res. 2010; 1314:194–205. [PubMed: 19782662]
3. Michel MC, et al. XVI. International Union of Pharmacology recommendations for the nomenclature of neuropeptide Y, peptide YY, and pancreatic polypeptide receptors. Pharmacol Rev. 1998; 50:143–150. [PubMed: 9549761]
4. Yulyaningsih E, Zhang L, Herzog H, Sainsbury A. NPY receptors as potential targets for anti-obesity drug development. Br J Pharmacol. 2011; 163:1170–1202. [PubMed: 21545413]
5. Sousa DM, Herzog H, Lamghari M. NPY signalling pathway in bone homeostasis: Y1 receptor as a potential drug target. Curr Drug Targets. 2009; 10:9–19. [PubMed: 19149531]
6. Antal-Zimanyi I, et al. Pharmacological characterization and appetite suppressive properties of BMS-193885, a novel and selective neuropeptide $Y_1$ receptor antagonist. Eur J Pharmacol. 2008; 590:224–232. [PubMed: 18573246]
7. Leibowitz SF, Sladek C, Spencer L, Tempel D. Neuropeptide Y, epinephrine and norepinephrine in the paraventricular nucleus: stimulation of feeding and the release of corticosterone, vasopressin and glucose. Brain Res Bull. 1988; 21:905–912. [PubMed: 3224284]
8. MacNeil DJ. NPY Y1 and Y5 Receptor Selective Antagonists as Anti-Obesity Drugs. Curr Top Med Chem. 2007; 7:1721–1733. [PubMed: 17979781]
9. Reubi JC, Gugger M, Waser B, Schaer JC. $Y_1$-mediated effect of neuropeptide Y in cancer: breast carcinomas as targets. Cancer Res. 2001; 61:4636–4641. [PubMed: 11389101]
10. Keller M, et al. $N^{\omega}$-Carbamoylation of the Argininamide Moiety: An Avenue to Insurmountable NPY $Y_1$ Receptor Antagonists and a Radiolabeled Selective High-Affinity Molecular Tool ($[^3H]$UR-MK299) with Extended Residence Time. J Med Chem. 2015; 58:8834–8849. [PubMed: 26466164]
11. White JF, et al. Structure of the agonist-bound neurotensin receptor. Nature. 2012; 490:508–513. [PubMed: 23051748]
12. Yin J, et al. Structure and ligand-binding mechanism of the human $OX_1$ and $OX_2$ orexin receptors. Nat Struct Mol Biol. 2016; 23:293–299. [PubMed: 26950369]
13. Yin J, Mobarec JC, Kolb P, Rosenbaum DM. Crystal structure of the human $OX_2$ orexin receptor bound to the insomnia drug suvorexant. Nature. 2015; 519:247–250. [PubMed: 25533960]
14. Shihoya W, et al. Activation mechanism of endothelin $ET_B$ receptor by endothelin-1. Nature. 2016; 537:363–368. [PubMed: 27595334]
15. Ballesteros, JA., Weinstein, H. Methods in Neurosciences. Sealfon, S., editor. Vol. 25. Elsevier; 1995. p. 366-428.

16. Kaiser A, et al. Unwinding of the C-terminal Residues of Neuropeptide Y is critical for $Y_2$ Receptor Binding and Activation. Angew Chem Int Ed Engl. 2015; 54:7446–7449. [PubMed: 25924821]
17. Venkatakrishnan AJ, et al. Molecular signatures of G-protein-coupled receptors. Nature. 2013; 494:185–194. [PubMed: 23407534]
18. Rasmussen SG, et al. Crystal structure of the $\beta_2$ adrenergic receptor-Gs protein complex. Nature. 2011; 477:549–555. [PubMed: 21772288]
19. Standfuss J, et al. The structural basis of agonist-induced activation in constitutively active rhodopsin. Nature. 2011; 471:656–660. [PubMed: 21389983]
20. Sautel M, et al. Neuropeptide Y and the nonpeptide antagonist BIBP 3226 share an overlapping binding site at the human $Y_1$ receptor. Mol Pharmacol. 1996; 50:285–292. [PubMed: 8700135]
21. Keller M, et al. Guanidine-acylguanidine bioisosteric approach in the design of radioligands: synthesis of a tritium-labeled $N^G$-propionylargininamide ([$^3$H]-UR-MK114) as a highly potent and selective neuropeptide Y $Y_1$ receptor antagonist. J Med Chem. 2008; 51:8168–8172. [PubMed: 19053784]
22. Sjodin P, et al. Re-evaluation of receptor-ligand interactions of the human neuropeptide Y receptor Y1: a site-directed mutagenesis study. Biochem J. 2006; 393:161–169. [PubMed: 16097949]
23. Poindexter GS, et al. Dihydropyridine neuropeptide Y $Y_1$ receptor antagonists. Bioorg Med Chem Lett. 2002; 12:379–382. [PubMed: 11814801]
24. Poindexter GS, et al. Dihydropyridine neuropeptide Y $Y_1$ receptor antagonists 2: bioisosteric urea replacements. Bioorg Med Chem. 2004; 12:507–521. [PubMed: 14723969]
25. Pedragosa-Badia X, Stichel J, Beck-Sickinger AG. Neuropeptide Y receptors: how to get subtype selectivity. Front Endocrinol (Lausanne). 2013; 4:5. [PubMed: 23382728]
26. Bender BJ, et al. Protocols for Molecular Modeling with Rosetta3 and RosettaScripts. Biochemistry. 2016; 55:4748–4763. [PubMed: 27490953]
27. Merten N, et al. Receptor subtype-specific docking of $Asp^{6.59}$ with C-terminal arginine residues in Y receptor ligands. J Biol Chem. 2007; 282:7543–7551. [PubMed: 17204471]
28. Xu B, et al. Mutagenesis and computational modeling of human G-protein-coupled receptor Y2 for neuropeptide Y and peptide YY. Biochemistry. 2013; 52:7987–7998. [PubMed: 24111902]
29. Lindner D, Walther C, Tennemann A, Beck-Sickinger AG. Functional role of the extracellular N-terminal domain of neuropeptide Y subfamily receptors in membrane integration and agonist-stimulated internalization. Cell Signal. 2009; 21:61–68. [PubMed: 18845246]
30. Laskowski RA, Swindells MB. LigPlot$^+$: multiple ligand-protein interaction diagrams for drug discovery. J Chem Inf Model. 2011; 51:2778–2786. [PubMed: 21919503]
31. Rosenbaum DM, et al. GPCR engineering yields high-resolution structural insights into $\beta_2$-adrenergic receptor function. Science. 2007; 318:1266–1273. [PubMed: 17962519]
32. Roth CB, Hanson MA, Stevens RC. Stabilization of the human $\beta_2$-adrenergic receptor TM4-TM3-TM5 helix interface by mutagenesis of $Glu122^{3.41}$, a critical residue in GPCR structure. J Mol Biol. 2008; 376:1305–1319. [PubMed: 18222471]
33. Kabsch W. Xds. Acta Crystallogr D. 2010; 66:125–132. [PubMed: 20124692]
34. McCoy AJ, et al. Phaser crystallographic software. J Appl Crystallogr. 2007; 40:658–674. [PubMed: 19461840]
35. Murshudov GN, et al. REFMAC5 for the refinement of macromolecular crystal structures. Acta Crystallogr D. 2011; 67:355–367. [PubMed: 21460454]
36. Smart OS, et al. Exploiting structure similarity in refinement: automated NCS and target-structure restraints in BUSTER. Acta Crystallogr D. 2012; 68:368–380. [PubMed: 22505257]
37. Emsley P, Lohkamp B, Scott WG, Cowtan K. Features and development of Coot. Acta Crystallogr D. 2010; 66:486–501. [PubMed: 20383002]
38. Keller M, et al. Mimicking of Arginine by Functionalized $N^{\omega}$-Carbamoylated Arginine As a New Broadly Applicable Approach to Labeled Bioactive Peptides: High Affinity Angiotensin, Neuropeptide Y, Neuropeptide FF, and Neurotensin Receptor Ligands As Examples. J Med Chem. 2016; 59:1925–1945. [PubMed: 26824643]

39. Cheng Y, Prusoff WH. Relationship between the inhibition constant ($K_I$) and the concentration of inhibitor which causes 50 per cent inhibition ($I_{50}$) of an enzymatic reaction. Biochem Pharmacol. 1973; 22:3099–3108. [PubMed: 4202581]
40. Burkert K, et al. A Deep Hydrophobic Binding Cavity is the Main Interaction for Different $Y_2R$ Antagonists. ChemMedChem. 2017; 12:75–85. [PubMed: 27874262]
41. Els S, Beck-Sickinger AG, Chollet C. Ghrelin receptor: high constitutive activity and methods for developing inverse agonists. Methods Enzymol. 2010; 485:103–121. [PubMed: 21050913]
42. Kostenis E. Is $G\alpha_{16}$ the optimal tool for fishing ligands of orphan G-protein-coupled receptors? Trends Pharmacol Sci. 2001; 22:560–564. [PubMed: 11698099]
43. Pedragosa-Badia X, et al. Pancreatic polypeptide is recognized by two hydrophobic domains of the human $Y_4$ receptor binding pocket. J Biol Chem. 2014; 289:5846–5859. [PubMed: 24375409]
44. Hoffmann S, Rist B, Videnov G, Jung G, Beck-Sickinger AG. Structure-affinity studies of C-terminally modified analogs of neuropeptide Y led to a novel class of peptidic $Y_1$ receptor antagonist. Regul Pept. 1996; 65:61–70. [PubMed: 8876037]
45. Gerald C, et al. A receptor subtype involved in neuropeptide-Y-induced food intake. Nature. 1996; 382:168–171. [PubMed: 8700207]
46. Schmidt P, et al. A reconstitution protocol for the in vitro folded human G protein-coupled Y2 receptor into lipid environment. Biophys Chem. 2010; 150:29–36. [PubMed: 20421142]
47. Casiraghi M, et al. Functional Modulation of a G Protein-Coupled Receptor Conformational Landscape in a Lipid Bilayer. J Am Chem Soc. 2016; 138:11170–11175. [PubMed: 27489943]
48. Hohwy M, Rienstra CM, Jaroniec CP, Griffin RG. Fivefold symmetric homonuclear dipolar recoupling in rotating solids: Application to double quantum spectroscopy. J Chem Phys. 1999; 110:7983–7992.
49. Raveh B, London N, Zimmerman L, Schueler-Furman O. Rosetta FlexPepDock *ab-initio*: Simultaneous Folding, Docking and Refinement of Peptides onto Their Receptors. PLoS One. 2011; 6:e18934. [PubMed: 21572516]
50. Song Y, et al. High-resolution comparative modeling with RosettaCM. Structure. 2013; 21:1735–1742. [PubMed: 24035711]
51. Schwarz D, et al. Preparative scale expression of membrane proteins in Escherichia coli-based continuous exchange cell-free systems. Nat Protoc. 2007; 2:2945–2957. [PubMed: 18007631]
52. Bosse M, et al. Assessment of a fully active class A G protein-coupled receptor isolated from in vitro folding. Biochemistry. 2011; 50:9817–9825. [PubMed: 21999704]
53. Wilkins MR, et al. Detailed peptide characterization using PEPTIDEMASS–a World-Wide-Web-accessible tool. Electrophoresis. 1997; 18:403–408. [PubMed: 9150918]

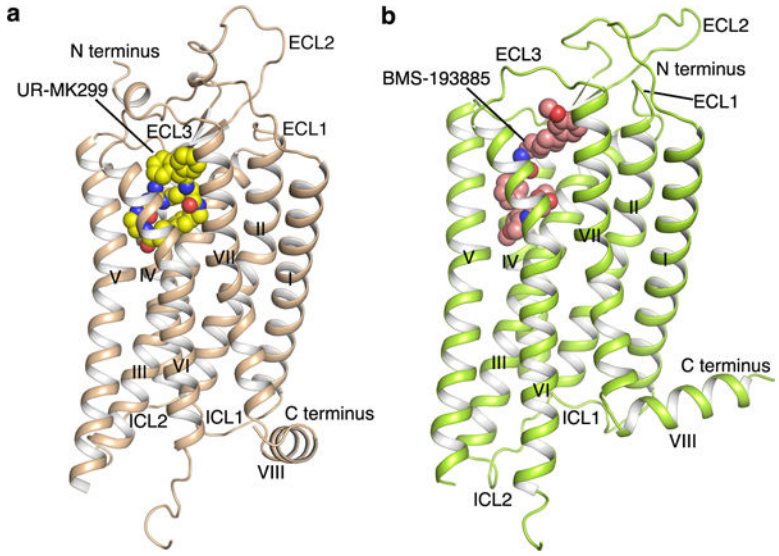


**Figure 1. Structures of $Y_1$R–UR-MK299 and $Y_1$R–BMS-193885 complexes**

**a**, Structure of $Y_1$R–UR-MK299 complex. The receptor is shown in brown cartoon representation. UR-MK299 is shown as spheres with yellow carbons. **b**, Structure of $Y_1$R–BMS-193885 complex. The receptor is shown in green cartoon representation. BMS-193885 is shown as spheres with pink carbons.

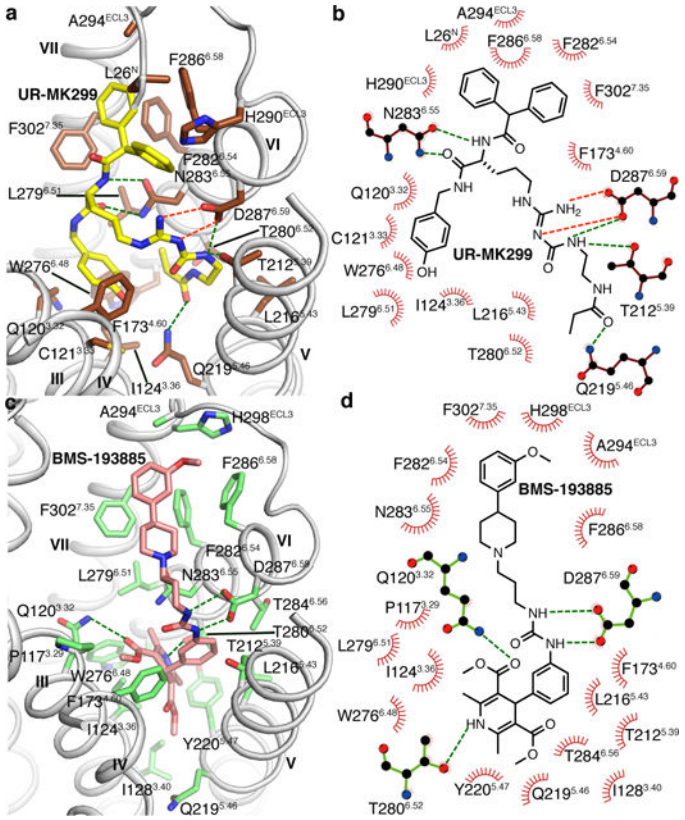


**Figure 2. Ligand-binding pocket of $Y_1R$ for UR-MK299 and BMS-193885**

**a**, Binding pocket for UR-MK299. The receptor is shown in grey cartoon representation. UR-MK299 (yellow carbons) and receptor residues (dark brown carbons) involved in ligand binding are shown as sticks. Salt bridge and hydrogen bonds are shown as red and green dashed lines, respectively. **b**, Schematic representation of interactions between $Y_1R$ and UR-MK299 analysed by LigPlot$^+$ (ref. 30). The stick drawing of $Y_1R$ residues is coloured dark brown. **c**, Binding pocket for BMS-193885. BMS-193885 (pink carbons) and receptor residues (green carbons) involved in ligand binding are shown as sticks. **d**, Schematic representation of interactions between $Y_1R$ and BMS-193885 analysed by LigPlot$^+$ (ref. 30). The stick drawing of $Y_1R$ residues is coloured green.

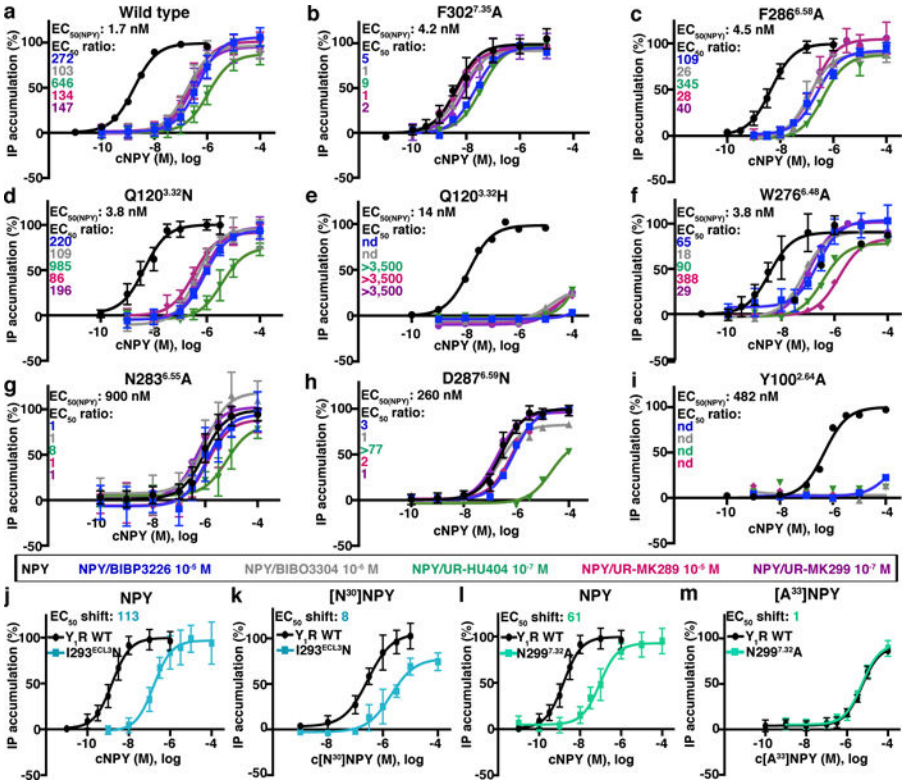


**Figure 3. IP accumulation assays**

**a-i**, NPY-induced IP accumulation of wild-type (WT) and mutant $Y_1$Rs in absence of antagonist or in presence of BIBP3226 ($10^{-5}$ M), BIBO3304 ($10^{-6}$ M), UR-HU404 ($10^{-7}$ M), UR-MK289 ($10^{-5}$ M) or UR-MK299 ($10^{-7}$ M). $EC_{50}$ values of NPY (black) and $EC_{50}$ ratios ($EC_{50(NPY+antagonist)}/EC_{50(NPY)}$) for antagonists (coloured) are given in the upper left corner for each plot. A reduced $EC_{50}$ ratio of mutant compared to the wild-type receptor was interpreted as important for the respective antagonist. nd, not determined. **j-m**, Complementary mutagenesis assays of [$N^{30}$]NPY with $I293^{ECL3}N$ (**j**, **k**) and [$A^{33}$]NPY with $N299^{7.32}A$ (**l**, **m**). $EC_{50}$ shifts ($EC_{50(mutant)}/EC_{50(WT)}$) are given in the upper left corner for each plot. A reduced $EC_{50}$ shift of NPY analogue/$Y_1$R mutant compared to NPY/$Y_1$R mutant was interpreted as no further loss of function and a direct interaction between both positions. At least two (n) independent experiments were performed in technical duplicate. If n>2, data are shown as mean ± s.e.m. If n=2, data shown are from a representative experiment. See Extended Data Table 2 for detailed statistical evaluation.

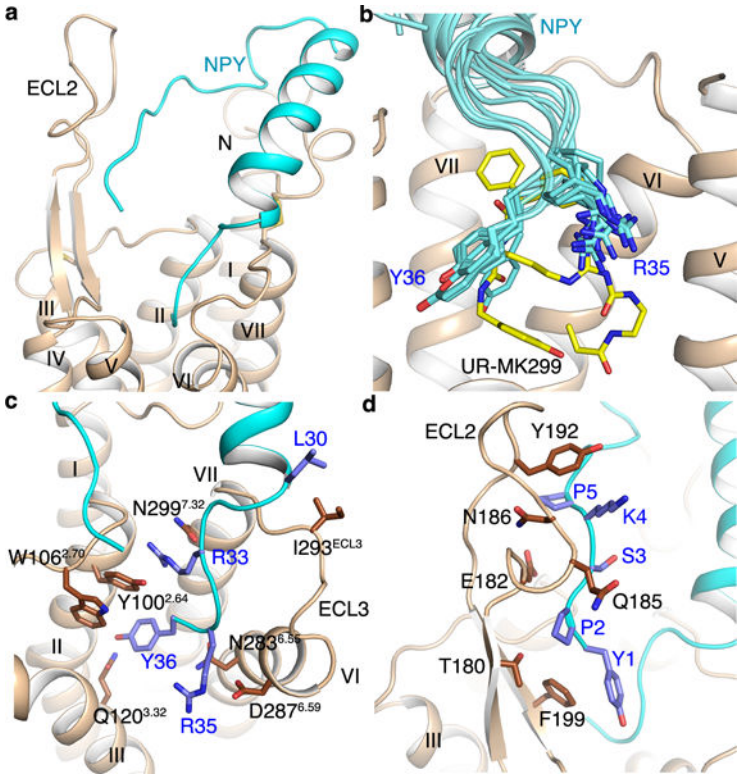


**Figure 4. Docking poses of NPY**

**a**, Predicted NPY binding pose. The receptor and the lowest energy NPY conformation are shown as cartoons, and coloured brown and cyan, respectively. **b**, Comparison of UR-MK299 (yellow sticks) binding mode and predicted ensemble binding mode of NPY residues R35 and Y36 (cyan sticks). **c**. Predicted binding mode between $Y_1R$ and NPY C terminus. Key Residues involved in $Y_1R$-NPY interaction are shown as sticks and coloured dark brown ($Y_1R$) and blue (NPY). **d**, Predicted binding mode between $Y_1R$'s ECL2 and NPY N terminus. Residues in $Y_1R$'s ECL2 and NPY N terminus that may form contacts are shown as dark brown and blue sticks, respectively.